ES Energy & Environment

REVIEW PAPER View Article Online

Pollutants Emissions of CO and Soot from Flame-wall Interactions in Fundamental and Practical Energy Conversion Systems: A Review

Minye Luo[1,2] and Dong Liu[1,2*]

Flame-wall interactions (FWI) as one kind of fundamental combustion phenomenon is universally found in various laboratory and practical combustion devices. It not only affects the combustion and energy conversion efficiency but also induces severe pollutants emissions. This review summarizes the pollutants emission characteristics in FWI from CO and soot aspects. The investigations of CO formation from FWI in various fundamental and practical energy conversion systems with different fuel types, operating conditions, sampling and analyzing methods and etc. are separately discussed. Meanwhile, multiple advanced laser diagnostics techniques are also adopted in different laboratory impinging flames to acquire more accurate and precise measurements of CO distributions in FWI. To gain more knowledge of pollutants emissions in FWI, the behaviors of soot from practical internal engines are observed with the aid of visualization techniques. Studies that utilize different combustion system configurations to modulate soot formation in FWI of practical engines are conducted as well. Recent literature subsequently evaluates the variations of soot morphology and nanostructure in FWI. The characteristics of soot particle size distribution function (PSDF) from FWI are briefly studied via burner-stabilized stagnation (BBS) flames at laboratory scale. The review ends with the unresolved issues for the future research.

Keywords: Flame-wall interaction; Pollutants emissions; Carbon monoxide; Soot particles

Received 19 November 2018**, Accepted** 24 December 2018

DOI: 10.30919/esee8c218

1. Introduction

The utilization of energy via various combustion devices played the pivotal role in the industrial and economical development. However, the growing depletion of fossil fuels combined with the severe environmental issues such as the global warming, particulate matter emission and air pollution urged people to pursue for the advanced combustion technology with the higher efficiency and the lower pollutants emissions. The profound understanding of the complicated combustion processes occurring in practical combustion devices was useful for researchers and engineers to design and optimize the devices with excellent combustion and emission performance. Flame-wall interactions (FWI) as one kind of fundamental combustion phenomenon were universally found in many technical combustors such as internal combustion engines, gas turbines and industrial furnaces and it could significantly affect the energy conversion efficiency and pollutants formation of combustors.[1]

FWI referred to the complex phenomenon involving physical and chemical influences when the flame directly contacted with walls.[2,3] The interactions between flame and walls could be distinguished into fluid-mechanism, thermal and chemical aspects based on different research interests.[4-6] Firstly, the flow structure would be disrupted by the wall and it fed back to flame characteristics such as the flame velocity which tended to be more notable in turbulence-dependent flames. Meanwhile, large heat fluxes were observed when the flame propagated toward the walls as the surfaces were prevalently much cooler than impinging flames. The significant heat losses to walls not only slowed the chemical reaction rates due to the lower flame temperatures but also affected the service life of device walls. In addition, the incomplete combustion occurred near the walls due to the lower reaction rates and the radical-radical recombination rates were promoted with the presence of walls. Consequently, the increasing emission levels of unburned hydrocarbons (UHC) and CO could be found. Especially, the formation and deposition of soot were found on the surface of walls in fuel-rich conditions. The deposition of soot exhibited the crucial influence on wall surface morphology and the flow and heat characteristics between the fluid and walls.[7] These facts explicitly depicted the influences of FWI on combustion and energy conversion efficiency and pollutants emissions. In order to optimize the combustion devices with better combustion and emission performance and develop the advanced combustion technology, the deeper insight and understanding of FWI are essential.

Nowadays, the investigation of FWI has been an attracting research field. It was not only the crucial subjects of research in safety technology,[8-11] enclosure fires,[12-17] catalytically assisted combustion,[18-22] materials synthesis,[23-26] and micro-combustion technology,[27-32] but also the topical concern of combustion chamber design of internal combustion engines,[33-36] gas turbines[37] and rocket engines.[38] Moreover, both of the

[1]*MIIT Key Laboratory of Thermal Control of Electronic Equipment, School of Energy and Power Engineering, Nanjing University of Science and Technology, Nanjing 210094, People's Republic of China*
[2]*Advanced Combustion Laboratory, School of Energy and Power Engineering, Nanjing University of Science and Technology, Nanjing 210094, People's Republic of China*
***E-mail:** dongliu@njust.edu.cn*

development of downsizing of engines in automotive and aircrafts which increased the surface-to-volume ratios[39] and the design of the innovative low-NO*x* gas turbine combustors[40,41] further emphasized the importance of FWI in combustion devices. In the past decades, considerable studies involving FWI were actively carried out. Most of the previous literatures were mainly focused on the flow field variations and heat transfer characteristics of FWI.[42-50] The experimental investigations of the heat transfer mechanism in FWI of laminar and turbulent flames with different parameters such as fuel types,[51-53] equivalence ratios,[54-56] Reynolds numbers,[57-59] nozzle to plate distances[60-62] and combustors configurations[63-65] have been extensively conducted to gain the comprehensive understanding of FWI thermal characteristics. Several numerical simulations were also carried out to establish empirical formulas and unveil the underlying thermal mechanism of FWI.[66,67] The relevant reviews of literatures on FWI heat transfer characteristics were also provided by Viskanta,[68] Baukal and Gebhart[69,70] and Chander and Ray.[71]

Despite the wide range of literatures on heat transfer properties of FWI, there were few publications concerning the influences of FWI on pollutants emissions. The formation of NO*x*, unburned hydrocarbons, CO and soot due to the incomplete combustion in FWI significantly reduced the combustion efficiency and caused the serious environmental and health issues. The soot production exacerbated the particulate matter emissions and the deposition of soot intensified the mechanical abrasion. Facing to the more stringent emission regulations, the pursuit of the higher efficiency and the lower harmful emissions needed the increased understanding of pollutants emissions in FWI. Meanwhile, the comprehensive information of pollutants emission characteristics in FWI would also be a valuable assistance to industrial engineers and researchers in this field. To the best of our knowledge, there has been little work to summarize the pollutants emissions in FWI. The objective of this review is to systemically analyze various pollutant emission characteristics such as CO, NO*x* and soot in FWI from fundamental and practical energy conversion systems.

2. CO emissions in flame-wall interactions

Carbon monoxide as one kind of significant gaseous emissions was produced due to the scarce of oxygen in the core reaction zones. The release of CO from flames could be a crucial criterion for many combustion system designs. In case of the domestic cooking, the level of CO emission from the FWI in stove-pot system was important to householders due to the poisoning of CO. Quantitative measurements of CO emissions in FWI of practical combustion systems, such as internal engines, were very difficult due to the complicated combustion processes, uncontrolled inflow and boundary conditions, and the small characteristic scales of space and time. The generic experimental setups which consisted of an impinging plate uprightly above burners were adopted to study the relevant physical and chemical properties of FWI in the laboratory flames. The different characteristics of CO emissions in FWI investigated by researchers were summarized in Table 1.

Table 1 Summary of types of fuel, oxidizer, flame and etc. adopted in investigations of CO emissions in FWI.

Reference	Fuel	Oxidizer	Type of flame	Reynolds number/velocity	Equivalence ratio (Φ)	Nozzle to plate distance (H/d)	Measured species	Sampling method
Wohr *et al*.[72]	Natural gas	Air	Partial premixed (RJRC)	7000	0.4-2.79	-	CO, CO_2, O_2, NO and NO*x*	Through a 3.9-mm-i.d. quartz probe which was placed in contact with the impinging plate and located at a certain radial distance.
Popp and Baum[73]	Methane	Air	Premixed	Laminar	Stoichiometric	-	Free radicals and intermediate species	-
Mishra[74]	LPG (70% butane and 30% propane)	Air	Premixed	2495 and 7161	1.2-4.0	0-20	CO, CO_2, O_2, NO and NO*x*.	The exhaust gas were collected by the 3.1 mm diameter water cooled stainless steel probe which was placed closer to the impingement surface at a radial location of r/d=25.0.
Sze *et al*[75]	Butane	Air	Inverse diffusion flames	1500-3000	1.0-2.4	0-160 mm	O_2, CO_2, CO and NO	Combustion gases were sampled from a 1 mm hole on the impinging plate.
Makmool *et al*.[76]	LPG	Air	Premixed	-	-	-	CO	A hood was above the burners to collect exhaust gases. A probe which connected to an emission analyzer was used to sample gases.
Saha *et al*.[77]	Methane, ethylene	Air	Premixed	310, 391, 515	2.57	1.0-5.0	CO, O_2 and NO*x*	The gases were measured by a probe at the outer edge of the target plate.
Li *et al*.[78]	LPG	Air	Premixed	500, 1000, 1500	0.9-1.2	3-7	CO and NO*x*	The gases were sampled via a circular hole with a diameter of 1 mm on the plate. The gases were ex tracted by a micro-pump at a 0.5 l/min.
Li *et al*.[79]	LPG	Air	Premixed	Q_{mix}=7.42x10^{-5}-1.11x10^{-4} m^3/s	0.9-1.2	3-6	CO and EICO	A sampling hole of 1 mm diameter was drilled on the plate to collect gas samples.

Table 1 (continued)

Reference	Fuel	Oxidizer	Type of flame	Reynolds number/velocity	Equivalence ratio (Φ)	Nozzle to plate distance (H/d)	Measured species	Sampling method
Zhen *et al*.[80]	LPG	Air	Inverse diffusion flames	2000-10000	1.0 to 2.0	12-132 mm	CO, NO*x*, EICO and EINO*x*	A small hole of 1 mm diameter was used to sample in-flame gases to acquire local pollutants. A hood method was adopted to collect exhaust gases to gain the overall pollutants.
Choy *et al*.[81]	LPG	Air	Inverse diffusion flames	Fuel flow rate of 1.39 x 10^{-5} m^3s^{-1}	0.8-3.0	20-180 mm	EICO and EINO*x*	The flues gases at a distance of 50 mm away from the stagnation point of the impinging flame were sampled via a 1 mm diameter hole in the plate. The emission of open IDF was measured by the hood method.
Makmool *et al*.[82]	LPG	Air	Premixed	404	1.28	0.7-2.9	CO	The standard hood method was used to collect exhaust gases.
Muthukumar *et al*.[83]	LPG	Air	Premixed	Wattage ranges from 1.3 to 1.7 kw.	0.554-0.7	-	CO and NO*x*	The hood was placed above the burner to collect gases which were analyzed via gas analyzers.
Zhen *et al*.[84]	LPG	Air	Premixed	600 to 2400	0.8 to 1.5	-	CO	A sampling tube ring was set around the periphery of the pot and 4 cm above the bottom of the pot.
Tajik *et al*.[85]	Methane	Air	Diffusion	1000-30000	-	0.5-3	CO_2, CO, O_2 and NO*x*	-
Mishra *et al*.[86]	LPG	Air	Premixed	Power input from 5 kw to 10 kw.	0.54-0.72	-	CO and NO*x*	Hood method
Panigraphy *et al*.[87]	LPG	Air	Premixed	Thermal load from 1.0 kw to 17 kw.	0.4-0.8	-	CO	Hood method
Zhen *et al*.[88]	Biogas/H_2	Air	Premixed	400-800	0.8-1.6	5-60 mm	EICO and EINO*x*	Hood method
Wei *et al*.[89]	Biogas/H_2	Air	Premixed	1000	0.8-1.4	5-50 mm	EICO, EINO*x*, CO, OH, HCO, N_2O and NO	Hood method
Mishra *et al*.[90]	LPG	Air	Premixed	Power range of 1-3 kw	-	-	CO and NO*x*	Hood method

2.1 Variations of types fuel, oxidizer and flame in investigations of CO emissions from FWI

The adoption of fuel types, oxidizer and other relevant parameters significantly affected the CO emissions in FWI. In studies of CO emissions of FWI, the categories of fuels were various. It ranged from the simple hydrocarbon fuel of methane to complicated fuel mixtures of liquid petroleum gas (LPG). The blends of H_2 and biogas which composed of CO_2 and CH_4 in different proportions were also considered. The oxidizer adopted in most research was compression air due to the prevalent utilization of ambient air in practical combustion systems. The numerical study which aimed to analyze the effects of different wall temperatures on major and intermediate species formation was conducted via the laminar stoichiometric methane flames.[73] The extensive experimental data and the detailed chemical mechanism of methane flames contributed to studying and verifying species concentrations. The variations of CO and NO*x* emissions in premixed impinging flames fueled with methane and ethylene were comparably studied to show the influence of fuel types on emission characteristics from FWI.[77] In the evaluation of combustion performance of practical cooking burners with different novel configurations, CO emissions as the most important criteria were tested. The LPG was usually chosen as the basic fuel due to its widespread usage in the domestic cooking.[76,83,86] To investigate the effects of fuel composition on pollutants performance of premixed impinging flames, the biogas containing CH_4 and CO_2 with the volume ratio of 1:1 was adopted by Zhen *et al*..[88] Meanwhile, considering the better performance of hydrogen in improving the combustion behaviors of the biogas fuel, up to 50 % of hydrogen were also added in the mixing fuels.

Most experiments in above studies chose premixed flames instead of diffusion flames to alleviate the disturbance of soot in the measurements of CO. Meanwhile, some other flame types such as partial premixed and inverse diffusion flames (IDF) were also used. The partially premixed natural gas impinging flames which was achieved by the radial jet reattachment combustion (RJRC) nozzle was adopted by Mohr *et al*.[72] to investigate the influence of increasing fuel/air mixing ratio on CO production from FWI. The combustion species and heat

transfer characteristics of the inverse diffusion impinging flames burning butane were presented to study the detailed relationship between the heat transfer and pollutants emissions.[75] The work by Zhen *et al*.[80] comparably analyzed the effects of swirling and non-swirling flows on the overall CO and NO*x* emission characteristics of LPG impinging inverse diffusion flames.

In the investigations of CO emission properties in FWI, either methane or LPG was universally adopted as the test fuel and the premixed flame was also the conventional combustion mode used in these experiments. For impinging flames, these arrangements could produce the large amount of CO due to the incomplete combustion and avoid the disturbance of soot formed in luminous flames. However, the CO emissions of more complicated fuels from diffusion flames which were more prevalently found in practical combustors have not been systemically tested. The pollutants emission characteristics from diffusion flames with more complicated fuel composition which were similar to practical fuels should be studied.

2.2 Effects of equivalence ratios on CO emissions in FWI

The majority of experiments which adopted premixed flames analyzed the pollutants emission characteristics from FWI under different equivalence ratios conditions. The equivalences ratios ranged from fuel-lean (Φ=0.4) to fuel-rich (Φ=4.0) conditions. The pollutants emission performance of flames could be directly affected by variations of equivalence ratios because the dissociation of fuels was controlled by the flame temperature. The flame exhibited the highest flame temperature at nearly stoichiometric condition due to the complete combustion.

A summary of the effects of equivalence ratios on CO emissions which were studied by different researchers was given in Table 1. The discrepancy of CO concentration between the RJRC and Co-Ax nozzles tended to be larger at the stoichiometric condition than that at fuel-lean conditions.[72] The average concentrations of CO and NO from the impinging premixed flames were presented when equivalence ratios increased from 1.2 to 4 respectively.[74] Results showed that the emission level of CO increased while the NO level decreased when the equivalence ratios shifted to richer part due to the decrease of flame temperature. Li *et al*.[78,79] separately analyzed the variations of CO concentrations and the emission index of CO (EICO) from FWI of different burner configurations at equivalence ratios of 0.9 and 1.0. The noticeable augment of CO concentrations and EICO were observed with the increase of equivalence ratios. In the research of Zhen *et al*.,[80] the swirling IDF had the minimum value of EICO at equivalence ratio of 1.4 which located at the near stoichiometric condition. The production of CO turned to be larger when the equivalence ratio continued to increase. The phenomenon could be attributed to the quenching effects when the flame touched the plate. Zhen *et al*.[88] also made an experimental investigation of the influence of equivalence ratio on the variations of EICO and EINO*x* (emission index of NO*x*) from the impinging premixed flame. The tested equivalence ratios ranged from 0.8 to 1.6 with an interval of 0.2 including fuel-lean and fuel-rich situations. It showed that the production of CO decreased when equivalence ratio increased from 0.8 to the stoichiometric condition because of the more complete combustion. The minimum value of CO emission located at equivalence ratio of 1.2 because the higher flame temperature and the higher laminar burning velocity of the slightly fuel-rich condition accelerated CO oxidation. When the equivalence ratio persisted increasing, the augment of CO emission was observed because of the intensive quenching effect of the plate.

It was seen from the above literature that equivalence ratios as one kind of the important experimental parameters exhibited the significant influence on CO production in FWI. The variations of CO emissions from FWI of premixed impinging flames with different equivalence ratios could be divided into two parts. The CO concentration reduced when the equivalence ratio shifted from the fuel-lean to stoichiometric conditions due to the more complete combustion and the higher flame temperature which promoted the CO oxidation. An augment of CO emission was found as the equivalence ratio shifted to the fuel-rich condition because of the quenching effects of plate. Whereas, many possible equivalence ratios and the detailed variations of CO distributions in FWI are scarce. Moreover, most of the industrial flames prevalently operated with diffusion flames. Very few studies analyzed the CO emission in FWI via diffusion flames.

2.3 Effects of Reynolds numbers on CO emissions in FWI

The Reynold number which affected the mixture flow rates was also the crucial experimental factor in combustion. The effects of the broad range of Reynolds numbers including laminar and turbulent conditions on CO emission properties in FWI have been extensively investigated and summarized in Table 1. In the study of CO variations from methane and ethylene partially premixed impinging flames, Reynolds numbers ranged from 310 to 515 to alleviate the soot formation and the decrease of CO was found with the increase of Reynolds numbers.[77] The increase of CO concentration from premixed impinging flames was observed by Li *et al*.[78] when Re was increase from 500 to 1500. This phenomenon was attributed to the promotion of intermediate combustion species and the enhancement of the interaction between the flame and walls. Ref[80] offered the variations of CO emission index from the impinging swirling and non-swirling IDFs when Re increased from 2000 to 10000. For non-swirling IDFs, the value of EICO was observed to be ascended with Re due to the increase of the fuel supply. Whereas, the reverse trend of CO variation was found for swirling IDF with increasing Re. This phenomenon was because of the stronger fuel/air mixing and the higher turbulence level caused by the augment of Re. In the numerical investigation of CO and NO*x* emissions from radial jet reattachment combustion flames with various Reynolds numbers (Re = 1000 to 30000), the higher concentrations of CO and NO*x* were observed at the larger Re.[85] Zhen *et al*.[88] analyzed the pollutants emissions from impinging 60 % Bg_{50} – 40 % H_2 mixture premixed flames with different Reynolds number of 400, 600 and 800. The results showed that the decline of the value of EICO was found against the increase of Reynolds numbers. The increase of Reynolds numbers enhanced the conversion rate of CO to CO_2.

The variations of Reynolds numbers could significantly affect the CO formation properties in FWI and multiple literatures had been carried out on this phenomenon with different burner configurations. Meanwhile, the variations of other exhaust gases such as NO*x* and CO_2 were also included in these studies. The influences of Reynolds numbers on CO emission characteristics could be summarized into two aspects.

Firstly, the flow rates at the nozzle exit which increased with Re promoted the entrainment of ambient air. It subsequently impacted the formation of intermediate species of flames.

Secondly, the flame length also extended with the augment of Reynolds numbers. The increase of flame length could promote the interaction between the flame and walls which led to the formation of unburned products. It also induced the flame quenching at the plate surface.

The research above mainly studied the local or overall variations of CO emission with Reynolds numbers. More detailed work is needed to

analyze the substantial effects of Re on CO formation in FWI.

2.4 Effects of nozzle to plate distances on CO emissions in FWI

The nozzle to plate distance which referred to the separation distance between the impingement plate and the burner nozzle was one sort of the important experimental parameters that can significantly affect the flame structures and emission performances in FWI.

The variations of pollutants emissions in impinging flames with different nozzle to plate distances had been included in many studies.[74,77,79-82,88,89] In the analysis of the emission characteristics from the LPG premixed impinging flames with different separation distance between the flame jet and the plate (H/d), the emission level of CO was closer to each other for H/d = 10 and 12 and an obvious augment of CO concentration was observed when H/d increased to 14.[74] The study of Saha *et al.*[77] showed that both methane and ethylene flames produced more CO when H/d decreased because of the incomplete combustion in wall jet region. The concentration of NO*x* ascended with the H/d as the oxygen content and the gas residence time increased. The value of emission index of CO for single-, twin- and triple-nozzle flames which were measured by Li *et al.*[79] tended to be larger with the decrease of nozzle to plate distances. Zhen *et al.*[80] illustrated the EICO and EINO*x* variations with different heights for swirling and non-swirling IDFs at fixed Reynolds numbers and equivalence ratio. The variations of EICO value with nozzle to plate distances were different for swirling and non-swirling IDFs due to the different flame structures. Higher value of EICO was found when the inner reaction zone impinged and quenched on the plate surface. The influence of nozzle to plate distance on NO*x* and CO emissions from impinging IDFs was investigated by Choy *et al.*.[81] The EICO persisted to decrease when H increased from 80 to 180 mm. It was attributed to the extended residence time for CO oxidation. The increase of nozzle to plate distance declined the CO concentration from LPG premixed flames.[82]

It was seen from the previous research that the value of CO emission from the majority of premixed impinging flames tended to be larger at the lower nozzle to plate distance. The decrease of distance between the nozzle and the plate increased the contact area between the flame and the plate which enhanced the flame quenching effect and promoted the formation of CO. When the plate was ascended to the higher height, the free flame length turned to be longer and the conversion rate of CO to CO_2 increased due to the more air entrainment. The concentration of CO subsequently declined with the increase of nozzle to plate distance. The variations of nozzle to plate distance exhibited the significant influence on pollutants formation process in FWI.

2.5 Sampling and analyzing methods of CO emissions from FWI

In the studies of emission performance in FWI, the sampling method was crucial to acquire the accurate and explicit information of pollutants formation as the interaction between flame and walls occurred in the very tiny space comparing to the conventional combustion. It also determined the accurate and elaborate distributions of pollutant gases such as CO, CO_2 and NO*x*. The sampling gases were generally tested via various gas analyzers in these studies. Fig. 1 exhibited that the sampling methods used in these literatures could be universally categorized into sampling probe,[72,74,77] micro-hole[75,78,79] and hood[76,82,83,87-90] methods.

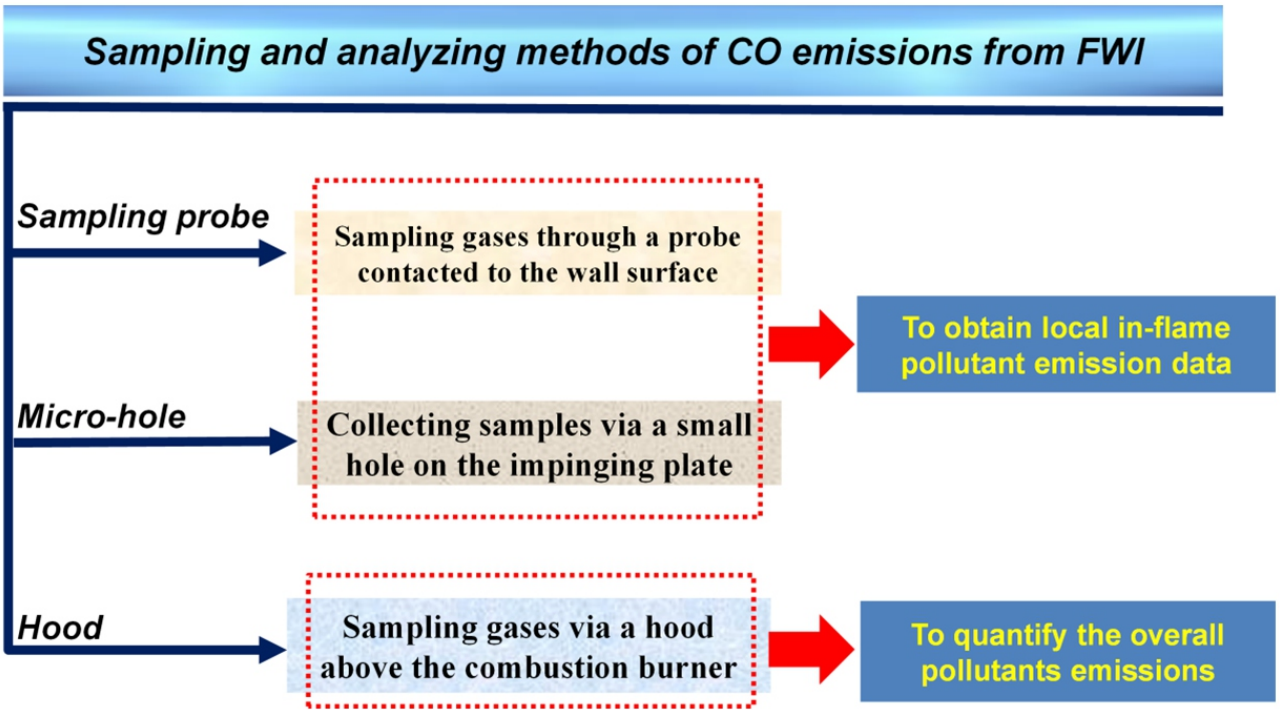

Fig. 1 The diagram of sampling and analyzing methods adopted in CO measurements from FWI.

In early days, the sampling probe method which set the probe close to the plate surface was utilized by researchers to collect and analyze gas specimen in the impinging flame layers. In order to study the exhaust gases from the RJRC nozzle, a quartz gas sampling probe was adopted by Mohr *et al*.[72] and it was placed in contact with the impinging plate to collect the exhaust gases. The probe was iso-kinetic to avoid the chemical reactions of intermediate species. It was located at the fixed radial distance to sample the gases flowing along the plate surface. Then the gases were analyzed through CO, CO_2, O_2, NO and NO*x* gas analyzers. The accuracy of gas sample was ± 0.5% full scale. Mishra *et al*.[74] set a water cooled stainless steel probe with 3.1 mm diameter close to the impingement plate surface to sample gases. The probe was located at the radial position of r/d = 25 where the outer edge of the flame. Meanwhile, the other three circumferential locations at the same distance were also measured to acquire the average values. The similar method was used in the work of Saha *et al*.[77] to analyze the emission characteristics after flame impingement. The stainless steel probe was arranged at the outer edge of the plate to measure CO and NO*x* concentrations when methane and ethylene flames impinged on the flat plate respectively.

Even though the probing method could acquire local in-flame pollutant emission data of the impinging flames, the dimension of probe might disturb the interplay between flames and walls and limited the profound investigation of pollutant gases distributions in flames. In order to overcome these limitations, Sze *et al*.[75] drilled a hole of 1 mm in diameter on the copper impinging plate and sampled combustion products. The burner was moved in the radial direction from 0 to 50 mm. The CO, CO_2 and O_2 distributions along the radial direction up to 50 mm with an interval of 1 mm were acquired. Li *et al*.[78] studied the emission characteristics in FWI via a premixed LPG flames uprightly impinged on a flat plate. The exhaust gases in impinging flames were collected through a circular hole with 1 mm diameter on the plate. These gas samples were extracted through a micro pump with the flow rate of 0.5 l/min and then analyzed through gas analyzers. Several positions along the radial direction were tested to obtain gases distributions in the impinging flame layer. The same group[79] also collected the relevant gases samples through the micro hole on the plate at the fixed location to evaluate the influences of nozzle diameter and arrangements on emission performance of impinging premixed flames.

Collecting gases samples through the micro-hole on the impingement surface provided the insight understanding of CO and NO*x* distributions in the flame layer close to the plate surface. Some researchers also proposed another method of comparing the emission performance from impinging and free flames to highlight the effects of FWI on pollutant formations. A sampling method via a hood device was used here. A standard hood method set a hood which was large enough to enclose the whole combustors above the burner to collect the flue gases. In this way, the impinging flame and the plate were considered as an entire system and exhaust gases from it could be totally collected by the hood. The collecting pollutants which were well-mixed mixtures were measured by various gas analyzers.[88] Makmool *et al*.[76] conducted CO emission test of four kinds of cook-top burners. The exhaust gases was collected via the hood device and analyzed through the CO analyzer. Makmool *et al*.[82] continued to systematically study the effects of height and inter-port spacing on heat transfer and emission performances of laminar impinging multiple premixed LPG flames. The CO emission in experiments was collected and measured by the hood method. In the investigation of Muthukumar *et al*.,[83] they chose the hood appliance combined with gas analyzers to examine CO and NO*x* emissions from novel porous radiant burners.

Collecting exhaust gases via the hood appliance was used to quantify the overall pollutants emissions from impinging flames. Some researchers proposed the combination of the hood and micro-hole methods to comparably investigate pollutants formation processes in FWI. Zhen *et al*.[80] analyzed variations of CO and NO*x* concentrations from impinging swirling and non-swirling inverse diffusion flames from two aspects. The local pollutants concentrations in flame layers were measured through the small hole on the impingement plate. Meanwhile, the sampling probe of gas analyzers was connected to the outlet of the hood which was arranged over the burner to acquire the overall emission index of CO and NO*x* from impinging swirling and non-swirling IDFs. In the experimental study of pollutants emission from impinging and open inverse diffusion flames carried out by Choy *et al*.,[81] they used two different sampling methods to collect exhaust gases from two kinds of combustors separately. For impinging IDFs, the flue gases from the flame layer close to the impingement plate was sampled from the micro-hole with 1 mm diameter on the plate. For open IDFs, a hood which was set over the flame tip collected exhaust gases. Then a steel probe was inserted on the top of hood to sample gases. Both of sampled gases were measured by gas analyzers. The comparison between them revealed that impinging IDFs generated more NO*x*.

These sampling methods allowed researchers to quantitatively investigate the pollutant emissions in FWI. The micro-hole sampling method could offer the local pollutants distributions in impinging flame layers along the radial directions and the overall emission index of pollutants were obtained through the hood method. The combined measurements exhibited the explicit knowledge of CO and NO*x* formation process in FWI.

2.6 Variations of measured species in FWI investigations

In the studies of pollutants emissions in FWI, CO and NO*x* were the most conventional species which were concerned and investigated by the most researchers.[76,78,83-86,90] The concentrations of CO and NO*x* were measured by the relevant gas analyzers. Li *et al*.[78] presented the distributions of CO and NO*x* concentrations on the radial direction in impinging flames with variations of equivalence ratios, Reynolds numbers and cooling water temperatures. The concentrations of CO and NO*x* were chosen by Muthukumar and Shyamkumar[83] as the testing standards to evaluate the performance of different porous radiant burners (PRB). Mishra *et al*.[86] exhibited the CO and NO*x* concentrations from the novel PRB with variations of input power and equivalence ratios via portable flue gas analyzers.

Meanwhile, the emission index which represented the grams of pollutant emitted per kilogram of fuel burned was also introduced in some research to illustrate the variations of CO and NO*x* emission properties in FWI.[79-81,88] Li *et al*.[79] adopted the EICO to characterize the CO emission from the premixed LPG/air impinging flames with different operation conditions and found that EICO increased with the decrease of the nozzle diameter in the single-nozzle flames. The values of EICO and EINO*x* of impinging premixed flames were offered by Zhen *et al*.[88] to show the influence of different separation distances and hydrogen addition on pollutants characteristics in FWI respectively.

To further analyze the formation processes of CO and NO*x* in FWI, the concentrations of O_2 and CO_2 were measured as the supplement as well.[72,74,75,85] In the work of Mohr *et al*.,[72] it was found that the Co-Ax nozzle produced more CO than that from RJRC nozzle. The O_2 concentration variations showed that RJRC nozzle entrained the more air than the Co-Ax nozzle and the conversion of CO to CO_2 were more completed in RJRC nozzle. Tajik *et al*.[85] showed that the higher production of CO at the higher temperature was due to the enhanced

CO_2 dissociation. The concentrations of several radicals and intermediate species from flames were also presented to gain deep understanding.[73,82] The concentrations of intermediate species and free radicals were provided by Popp *et al*.[73] in the numerical study of the unburned hydrocarbons formation during the head-on quenching of the laminar methane flames. The distributions of OH radical at different separation distances in impinging flames were offered to show the intensive oxidation regions.[82]

The concentrations of CO and NO*x* were universally chosen as the emission standards to evaluate the pollutants emission performance in FWI. The concentration of O_2 and CO_2 sometimes were also measured as the supplement of emission characteristics and it helped to analyze the formation processes of CO and NO*x*. Whereas, the measurements of distributions of more major and intermediate species in the interaction between flame and walls were scarce except for several numerical simulations limited to the sampling and analyzing methods. The information of more species distributions in FWI under various operation conditions is needed to gain the deep understanding of pollutants characteristics in FWI.

Overall, in the experimental studies of pollutants emissions in FWI, the concentrations of CO and NO*x* were universally measured to evaluate the emission characteristics in FWI. The impinging flame device was generally adopted in the analysis of interaction between flame and walls. Researchers adopted the gaseous and light hydrocarbon fuels and premixed combustion mode to avoid the disturbance of soot. The effects of different experimental parameters including equivalence ratios, Reynolds numbers, nozzle to plate distances and etc. on CO formation process were investigated respectively (shown in Fig. 2). Meanwhile, the in-flame and overall pollutants emission properties from FWI were also acquired through the sampling probe, micro-hole and hood method separately. The above information could help to obtain the CO and NO*x* formation in FWI. Further investigation of CO distributions on the impinging flame layer near the wall surface and more species concentrations will be needed in the future work.

3. CO emissions measured via laser diagnostics techniques

In the usual studies of the influence of FWI on pollutants emission characteristics mentioned above, the concentrations of various combustion products such as CO, NO*x* and CO_2 were generally acquired via the gas analyzers. However, considering that the boundary layer where the FWI occurred was just in the scale of hundreds of microns, the limited resolution and the spatial dimension of conventional gas analyzers did not satisfy the standards of refined measurements. Nowadays, the advanced laser combustion diagnostics methods which had high spatial and temporal resolution were introduced to study the complex interactions between the flame and walls. The relevant review of the utilization of diverse laser techniques to diagnose complex combustion processes in laboratory and practical combutors had been presented by Dreizler *et al*..[1] It was seen that the laser-based techniques which possessed advantages including non-intrusive and in situ nature, temporal resolution and multi-parameter measurements were able to obtain the accurate and precise measurements in complicate combustion environments. A summary of the application of laser diagnostics in FWI such as planar laser induced fluorescence of the OH-radical (OH-LIF), Raman scattering and coherent anti-Stokes Raman spectroscopy (CARS) with various operating conditions was presented in Table 2.

3.1 Arrangements of fuel types, flame types and the plate position in FWI laser diagnostics studies

In the most studies which applied the laser diagnostics methods, the methane/air premixed flames were chosen as the fundamental flame because it had the simple chemical mechanism and less soot formation which might interfere the measurements of laser devices.[92-99,102,103] Several researchers also adopted some other complex gas fuels in the measurements of FWI via laser diagnostics techniques.[91,100,101] Mokhov *et al*.[91] measured the combustion products distributions along the plate surface in propane-air premixed flames. Except for the conventional

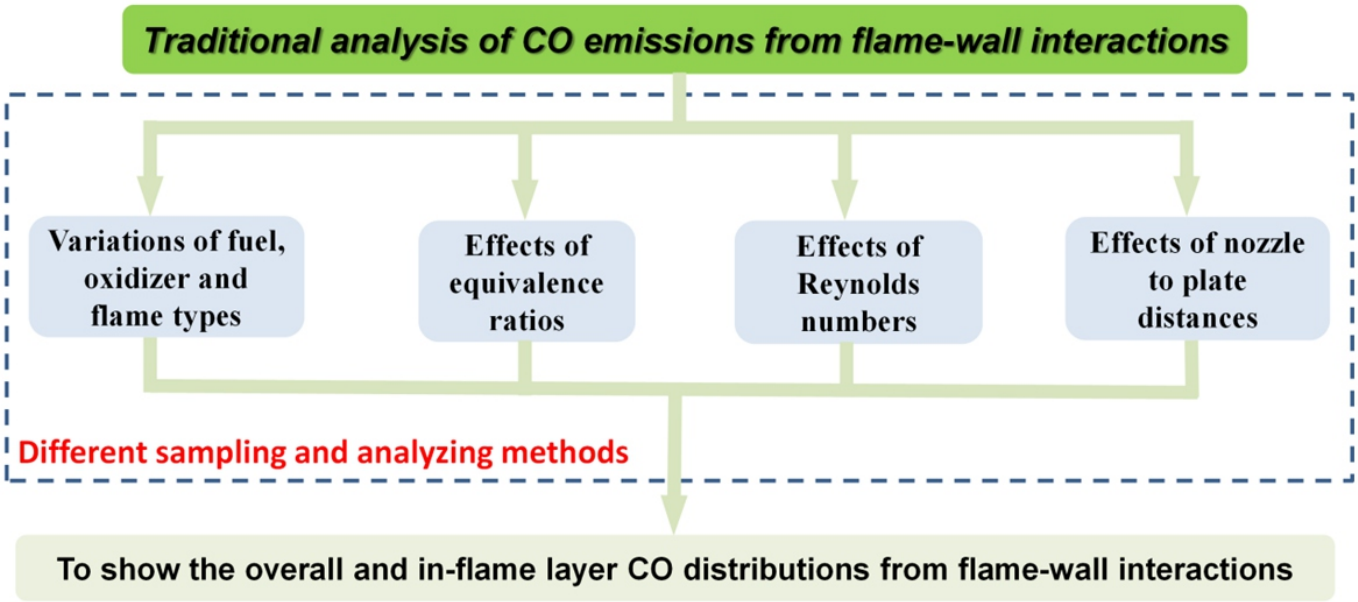

Fig. 2 The sketch of traditional analysis of CO emissions from flame-wall interactions.

methane/air premixed flames, Häber and Suntz[100] also conducted the experiments of the influence of wall materials on pollutants emissions in FWI of propane/air flames with a wide range of equivalence ratios as the supplement for the previous studies. In the investigation of Kosaka *et al*.,[101] they comparably analyzed the influence of wall temperatures on CO formation in stoichiometric methane and dimethyl ether (DME) flames separately. The utilization of DME which was a more complex fuel extended the previous research.

Most of the mentioned studies which investigated the CO emission from FWI via two-photon CO-LIF were under premixed or partially premixed flame conditions. In the work of Chien *et al*.,[95] they examined the CO emissions characteristics through methane diffusion impinging flames. Even though they used the methane diffusion flames, the Reynolds number of the flow rate was so small that few soot particles were found in the flames.

Fig. 3 showed that the arrangements of the impingement plate in experiments could be classified into head-on quenching (HOQ)[93-95,99] and side-wall quenching (SWQ).[91,92,96-98,100-103] Both of the HOQ and SWQ were two kinds of FWI which were usually found in practical combustors. The situation of HOQ presented the flame perpendicularly propagated toward the cold walls. It was achieved by the plate which was vertically set above the burner to form the stationary wall-stabilized flames. Unlike to the HOQ condition mentioned in section 2, researchers chose the convex wall instead of the flat plate to develop the laser measurement environment. Singh *et al*.[93] set a slight convex water-cooled stainless-steel wall above the burner. The convex wall which was part of a sphere offered the space for the implement of focused point–wise laser diagnostics to measure the CO concentrations in the near wall boundaries. The similar HOQ device was also used to investigate the behaviors of CO formation from FWI in stationary and propagating impinging flames respectively.[94] The distributions of temperature and CO mole fractions in steady-state and transient processes of FWI were presented respectively. In the investigation of the effect of the pressure on nitric oxide formation in premixed jet-wall stagnation flames, the experimental device of HOQ which could offer the compact and stable flames at the high pressure conditions was adopted.[99]

In the configuration of SWQ, the plate was set parallel to the flow rate direction which allowed the flame to propagate along the surface. The arrangement of SWQ could provide the persistent and stationary FWI in both laminar and turbulent flows in comparison to that of HOQ. In the early study of Mokhov *et al*.,[91] they directly placed the flat steel

Table 2 Comparisons of types of fuel, flame, plate location and other operating conditions in various literature involving laser diagnostics techniques.

Reference	Fuel	Type of flame	Plate location (HOQ/SWQ)	Reynolds number	Equivalence ratio (Φ)	Measured species	Analysis method
Mokhov *et al*.[91]	Propane	Premixed	SWQ	Laminar	0.83-1.0	CO and OH	OH-LIF, CO two-photon LIF
Fuyuto *et al*.[92]	Methane	Premixed	SWQ	Laminar	0.9	OH, CH_2O, CO, NO and H_2CO	NO-LIF, single-photon (OH, CH_2O) and two-photon (CO) excitation LIF
Singh *et al*.[93]	Methane	Premixed	HOQ	Laminar	0.83-1.2	CO	CO LIF
Mann *et al*.[94]	Methane	Premixed	HOQ	Re=5000	0.83-1.2	CO	Two-photon LIF
Chien *et al*.[95]	Methane	Non-premixed	HOQ	Laminar (Re=50)	-	CO	PLIF of OH and 2-photon CO
Ganter *et al*.[96]	Methane	Premixed	SWQ	Laminar		CO	-
Jainski *et al*.[97]	Methane	Premixed V-shaped flame	SWQ	Laminar and turbulent (Re=5000)	0.83-1.2	CO	Two-photon CO LIF
Bohlin *et al*.[98]	Methane	Premixed V-shaped flame	SWQ	Laminar and turbulent (Re=5000)	0.83-1.2	N_2, O_2, H_2, CO, CO_2 and CH_4	Ultrabroadband coherent anti-Stokes Raman spectroscopy (CARS)
Versailles *et al*.[99]	Methane	Premixed jet-wall stagnation flames	HOQ	Laminar	0.7	NO	NO-LIF
Häber *et al*.[100]	Methane, Propane	Premixed stagnation side-wall flames	SWQ	5000	0.76-1.35	OH* and CH*	Chemiluminescence imaging
Kosaka *et al*.[101]	Methane, DME	Premixed V-shaped flames	SWQ	Laminar and turbulent (Re=5000)	1	OH* and CO	Two-photon LIF
Ganter *et al*.[102]	Methane	Premixed flame	SWQ	Laminar (Re=5000)	1	CO	-
Heinrich *et al*.[103]	Methane	Premixed V-shaped flames	SWQ	Laminar (Re=5300)	1	CO and OH	-

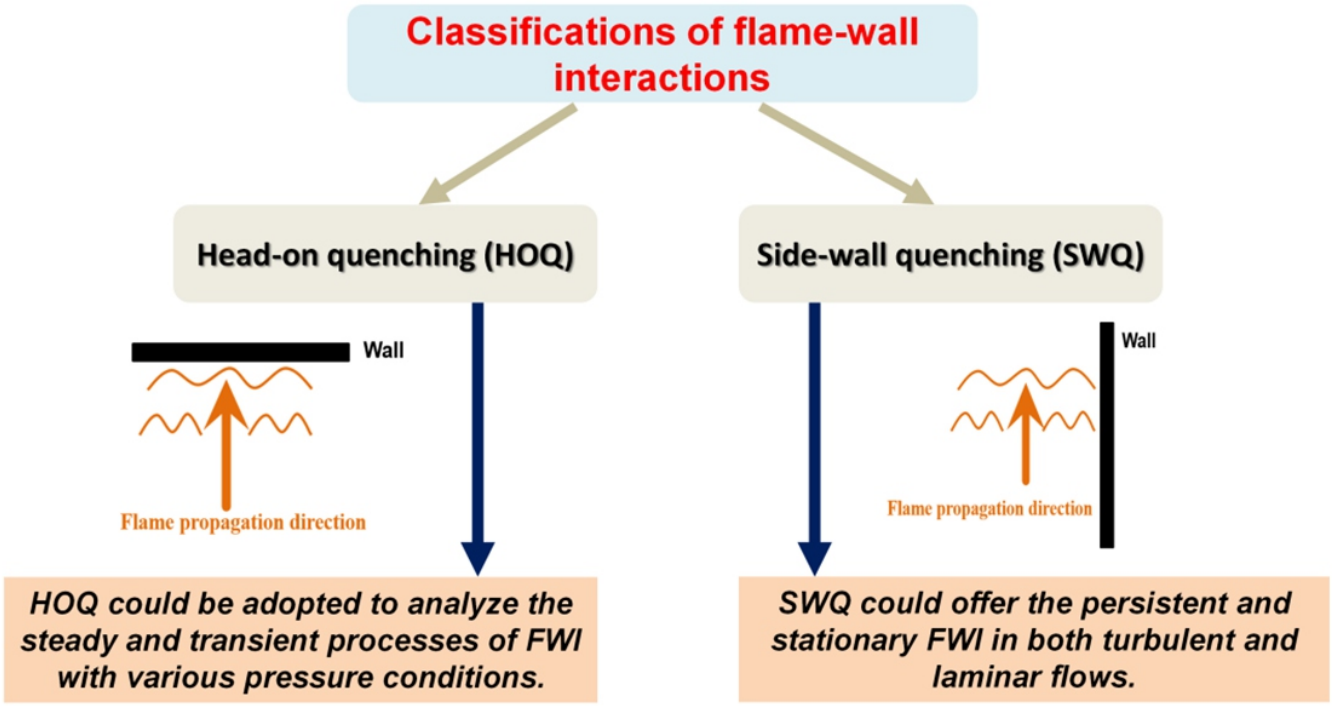

Fig. 3 Classification of flame-wall interactions.

plate into the combustion products flows above the burner to form flame-wall interactions. The edge of the plate was sharpened to reduce the disturbance of flows. Fuyuto *et al.*[92] developed a traditional SWQ device by putting a water-cooled stainless steel wall parallel to the main flow rate from a premixed methane/air flat flame burner. The flat flame front was divided into two parts and the FWI was found at the front wall surface. To further improve and control the interplay between the flame and walls in SWQ, the team of Dreizler[97,98,101,102] set a tiny circular ceramic rod above the burner to form a premixed V-shaped flame. One branch of the flame interacted with the vertically oriented stainless steel wall and developed the stable FWI. The interactions could be conveniently controlled by the adjustment of the location of the rod.

The relevant simulation models of SWQ were established to investigate the latent mechanism of pollutants formation in FWI. The two-dimensional (2D) laminar simulation model was developed by Ganter *et al.*[96] to numerically analyze the FWI in the premixed stoichiometric SWQ configuration. Various reaction mechanisms and diffusion treatments were comparably studied in the simulations. Heinrich *et al.*[103] continued to expand the calculation model and carry out a three-dimensional (3D) numerical simulation to analyze the FWI in SWQ configuration. The computational results including flow structures were also compared with the previous experimental data and two-dimensional simulations.

In the laser diagnostics of pollutants emission properties in FWI, the methane/air premixed flames which formed few soot particles and provided the steady flame were used as the fundamental flame. The configurations of HOQ and SWQ which were universally found in practical combustion appliances were detailedly analyzed. The HOQ device offered the way to study the emission characteristics in steady and transient FWI. Meanwhile, the SWQ device combined with the V-shaped flame provided the more stable and persistent FWI for laminar and turbulent conditions.

3.2 Effects of different operating conditions considered on FWI laser diagnostics

Except for developing the relevant laser diagnostics measurements in FWI in some studies, the effects of several experimental parameters including equivalence ratios, laminar and turbulent flow conditions and plate temperatures on pollutants emission characteristics were considered in the investigation of FWI through laser-based diagnostics techniques.[91-95,97-99,101]

The distributions of CO in impinging flame layers with different equivalence ratios which presented the significant influence on the overall CO emission characteristics from FWI were explicitly analyzed. In the study of OH and CO behaviors in the boundary layer near wall surface, the influence of different experimental factors including equivalence ratios which ranged from 0.83 to 1.0 and plate temperatures (cooled and uncooled) was considered.[91] It was found that the production of CO obviously decreased with the decrease of equivalence ratio at the ranging of near stoichiometric. The augment of the plate surface temperature also inhibited the CO formation in the boundary layer. Jainski *et al.*[97] combined the advanced laser diagnostic methods and the side-wall quenching device to study the FWI in atmospheric premixed laminar flame. The performance of the quenching distance which was an important quantity of FWI was evaluated at equivalence ratio of 0.83, 1.0 and 1.2. They also comparably analyzed the influence the laboratory-fixed and the flame-fixed coordinate systems on thermochemical states which presented more details in FWI through the CO/T-state diagrams. In the study of Bohlin *et al.*,[98] the temperature distributions in the near-wall region with different equivalence ratios were investigated by the one-dimensional coherent anti-Stokes Raman spectroscopy.

Reynolds numbers as another important experimental factor were also investigated by many researchers. The distributions of flame temperatures and species of the near-wall layer in a quenched FWI were

reported by Fuyuto *et al.*[92] via the planar LIF with gas flow rates of 7.5 and 15 l/min separately. Kosaka *et al.*[101] investigated the characteristics of CO formation and oxidation processes in FWI of a side-wall quenching device under laminar and turbulent conditions. The Reynolds numbers were set 5000 for both the laminar and turbulent parameters. The turbulent flame was achieved via an inserted turbulence grid. The results showed that the branch of CO formation and oxidation shifted to the lower temperature region due to the impact of turbulence.

Several researchers simultaneously investigated pollutants emission characteristics in FWI with the combination of equivalence ratios and Reynolds number variations. The variations of temperature and CO distributions in FWI with different equivalence ratios and Reynolds numbers were reported by Singh *et al.*[93] It was observed that the profiles of CO mole fraction were similar at equivalence ratio of 0.83 and 1.0 and the reduction of CO concentration mainly located in the hot flame region. In case of the fuel rich flame, the mole fraction of CO almost kept constant in the post-flame region. The peak value of CO mole fraction declined and the position of the flame front shifted to the wall surface with the increase of Re. Mann *et al.*[94] presented variations of CO mole fraction in FWI from the atmospheric methane jet impinging flames for different equivalence ratios which ranged from 0.83 to 1.2 and two turbulence intensities. The conditional statistics analysis method was used to acquire the difference of thermos-chemical states between the stationary impinging flames and the flames during head-on quenching from 200 individual experimental data. The higher CO concentration was found at the lower temperature region due to the inhibition of CO oxidation of enthalpy losses. This phenomenon was more significant in fuel lean flames.

Except for changes of equivalence ratios and Reynolds numbers, effects of other relevant experimental parameters on pollutants formation in FWI were also considered. The distributions of CO released from the non-premixed methane impinging flames with different nozzle to plate distances were analyzed by Chien *et al.*.[95] The relationship between the reaction zone and the heat release zone was established. Versailles *et al.*[99] examined the formation processes of NO in the methane/air jet-wall premixed flames and the influence of the operating pressure was also studied. The very limited and negative effect of pressure on the production of nitric oxide was found in fuel-lean flames.

The effects of various experimental parameters including equivalence ratios and Reynolds numbers which were similar to those in section 2 on pollutants emission characteristics from FWI were analyzed via the HOQ and SWQ devices. The utilization of the advanced laser diagnostics methods helped to gain the well spatially resolved measurements of temperature and intermediate species within the subtle boundary layer near the wall surface. These results also corresponded with the consequences acquired by gas analyzers in some cases.

3.3 Development of various laser diagnostics methods in FWI

The progressive development of laser diagnostics techniques helped researchers to gain the better understanding of combustion science and technology. The role and evolvement of laser diagnostics in FWI were summarized and presented in Fig. 4.

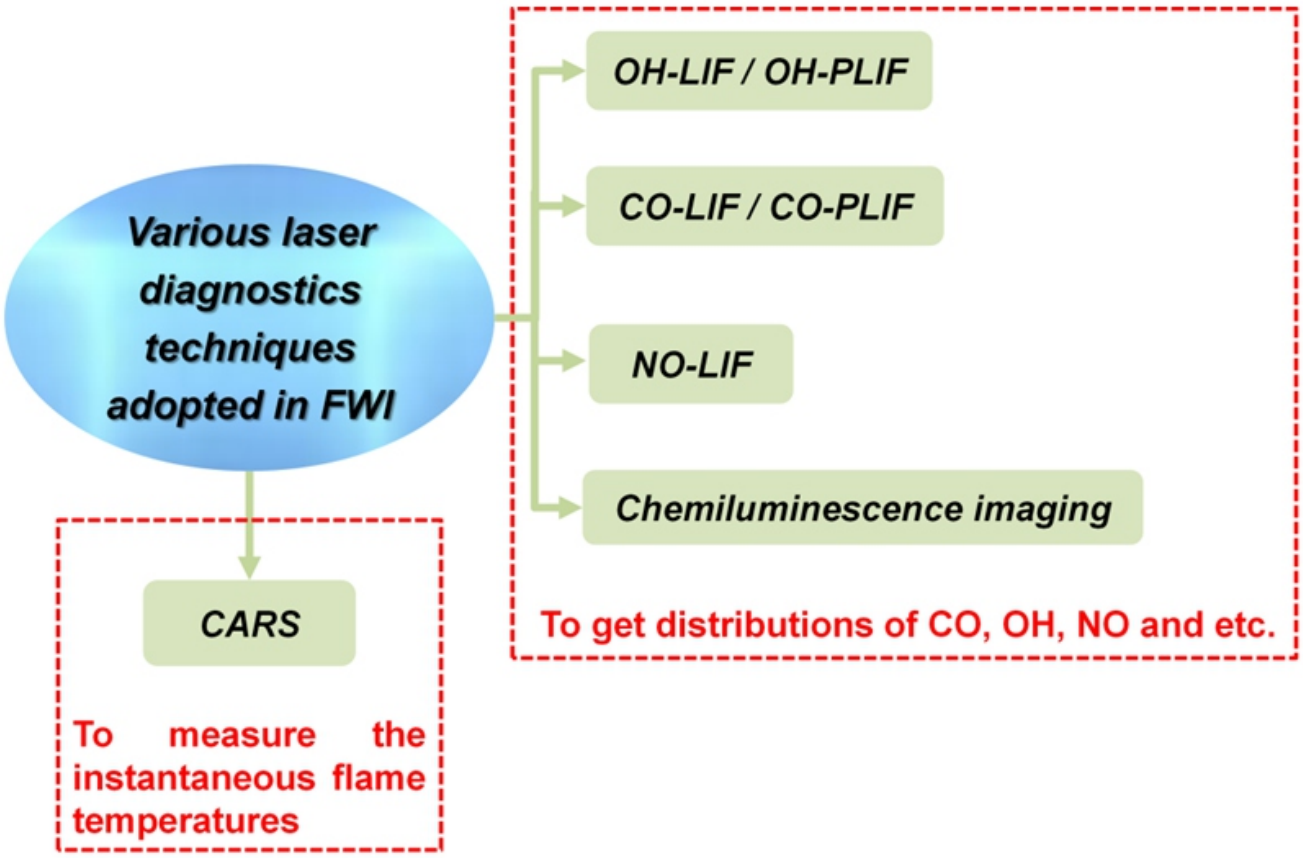

Fig. 4 The illustration of various laser diagnostics techniques used in FWI.

The laser-induced fluorescence technique was universally adopted in the measurements of OH and CO distributions from FWI. In the work of Mokhov *et al*.,[91] they measured the number density of OH in the boundary layer near the wall region through the absorption and laser-induced fluorescence. The spatial resolution for the boundary layer was 0.25 mm and the random error was about 10%. The concentration of CO was acquired by the two-photon LIF and the accuracy of the measured boundary layer was 0.1 and 0.2 mm for the uncooled and cooled plate separately. The gas-phase temperature distributions in the boundary layer at atmospheric pressure were measured by Fuyuto *et al*.[92] with the help of multi-line NO-LIF thermometry in the investigation of FWI. Moreover, more intermediate and major species containing OH, CH_2O and CO were measured in flames through single-photon (OH, CH_2O) and two-photon (CO) excitation LIF. The imaging system had the well spatial line-pair resolution of 22 μm and the accuracy of the temperature measurement in the near-wall region was within 50 K. The measurement range of the applied laser diagnostics devices could be as close to the wall surface as 200 μm. In the study of Chien *et al*.,[95] they illustrated the predominant factors that affected the CO formation and emission from an impinging flame. The relevant distributions of OH and CO in flames were acquired with the utilization of OH-PLIF and CO two-photon PLIF.

Considering the importance of flame temperature distributions in combustion processes, the development of CARS offered researchers an access to measure the instantaneous flame temperatures in FWI. In the analysis of the FWI by laser based techniques conducted by Singh *et al*.,[93] the combination of two-photon laser-induced fluorescence and coherent anti-Stokes Raman spectroscopy could simultaneously offer the distributions of gas phase temperatures and CO. The data of temperature was used to correct the CO concentration acquired from the CO-LIF. In the examination of temperature distributions and CO variations in the transient FWI, the instantaneous temperatures were gained by the nanosecond CARS device.[94] Jainski *et al*.[97] also measured the CO concentrations and temperatures by CO-LIF and CARS. The velocity fields and flame structures were obtained by two-component particle image velocimetry (PIV) and OH-PLIF. The CO/T-state diagrams were also established to analyze thermochemical properties.

Except for the measurements of temperatures and CO mole fractions, more combustion products including N_2, O_2, H_2, CO_2 and CH_4 were detected in the one-dimensional-CARS imaging configuration.[98] The resolution of the imaging was better than 40 μm and the boundary layer was measured to be approximately 30 μm. Versailles *et al*.[99] also studied the NO formation process in FWI and the concentrations of NO and N_2O were detected by NO-LIF. To investigate the FWI in SWQ configuration, Häber *et al*.[100] evaluated the quenching distances through chemi-luminescence images of OH* and CH* radicals.

The adoption of advanced laser diagnostics techniques in investigations of FWI offered the more accurate and precise spatial resolution of flame species near the wall region. Meanwhile, the scope of the boundary layer which contacted to the wall surface could be much thinner to capture more details in the interplay between the flame and walls. The combination of CO-LIF and CARS also offered the opportunity to detect the carbon monoxide and temperature at the same time and the concentration of CO could be timely modified according to the temperature data. Moreover, the variations of species and temperature distribution from persistent and transient FWI could be acquired with the help of laser diagnostics. The information of other combustion products measured in FWI also contributed to the deep insight of FWI processes.

The investigation of several combustion parameters in FWI via the combination of the advanced laser diagnostics techniques and HOQ/SWQ devices was the extension and supplement of the previous studies of FWI through gas analyzers. It also broke through the limitations of measurements of overall pollutants emissions in FWI and innovatively offered the useful qualitative or semi-quantitative information of species distributions in the subtle boundary layer which was in hundreds micron order near the wall surface. The influence of different universal experimental factors including equivalence ratios, Reynolds numbers and etc. on emission characteristics in FWI were analyzed. The mole fractions of major and intermediate species were acquired. Both of these information mentioned above facilitated the better understanding of FWI.

Despite these advantages of the utilization of advanced laser diagnostics in FWI mentioned above, there are several limitation and challenges to be resolved for present experimental investigations. For example, the measurements of combustion species are merely centered on the simple and major species such as CO, CO_2 and etc. The gas-phase temperatures which located near the wall surface are much higher than the wall surface temperatures due to the limited spatial resolution and the refraction effects of the LIF imaging system. Meanwhile, the useful results of species distributions are obtained at the distance of hundreds of micron scale from the wall instead of the substantial surface. Most of the experimental studies are carried out at the laboratory scale.

In the future work, the detection of combustion species through laser based diagnostics in FWI should contain more major and intermediate species even the large macromolecule polycyclic aromatic hydrocarbons (PAH). Much smaller distance and more precise measurements with higher spatially resolution should be acquired with the advances of laser devices. Several other external experimental parameters such as pressure and surface properties are also required to study to expand the database of FWI and the utilization of relevant advanced diagnostic strategies in more complex practical combustion systems.

4. Soot formation and emission in flame-wall interactions

The previous researchers explicitly investigated the pollutants emission performance in FWI via various laboratory flames. Both of the overall emission index and the spatial distributions of pollutants in the boundary layer near the wall surface were accurately obtained with the aid of various gas analyzers and the advanced laser based diagnostics techniques. The knowledge of pollutants formation processes helped researchers to understand the mechanism of FWI and develop strategies to improve energy utilization. Whereas, most of these studies were carried out in premixed combustion mode fueled with various simple gaseous hydrocarbon fuels. The investigation of the characteristics of pollutants from FWI in diffusion flames which universally appeared in different practical combustion appliances was scarce.

Moreover, the combination of heat losses to the wall and the free radicals quenching on the wall surface in FWI intensified incomplete combustion when the flame propagated toward combustor walls. More unburned hydrocarbons were formed in this process and it reduced the combustion and emission performance. Especially for soot formation which occupied the large percentage of particulate matter emissions not only did harm to human health and environmental issues but also induced the abrasion of combustor walls and decreased the energy utilization efficiency. The phenomenon was more serious in enclosed combustion systems which adopted diffusion flames such as internal combustion engines and industrial combustion furnaces.

Facing to the rigid emission regulations and the development of

Table 3 A summary of previous studies on soot behaviors from flame-wall interactions in practical combustion systems.

Reference	Fuel types	Variations in the study	Analysis method	Aim of the study
Gao *et al*.[104]	Diesel	Flame luminosity and OH radical	High-speed direct flame imaging and OH chemiluminescence imaging.	To investigate the effect of included angle on impinging flame structures and combustion performance.
Wang *et al*.[105]	JIS#2 Diesel	Soot luminosity and concentration	Two-color pyrometry and the high-speed imaging.	The influence of ultra-high pressure and micro-hole nozzle on soot formation from FWI.
Kiplimo *et al*.[106]	JIS#2 Diesel	Variation s of hy drocarbons, NO*x*, CO and soot	Emission gas analyzers, smoke meter and the relevant flame luminosity analysis.	The combustion and emission performance of the PCCI diesel engine with various spray impingement, injection parameters and EGR.
Rusly *et al*.[107]	ULSD	Natural soot luminosity and OH radical.	OH chemiluminescence imaging and high-speed flame imaging.	To comparably study the effects of jet-wall and jet-jet interactions on flame structures and soot luminosity.
Le *et al*.[108]	ULSD	Flame structure and soot luminosity.	OH-PLIF, fuel-PLIF and line-of-sight integrated chemiluminescence imaging.	Effects of flame-wall interactions on impinging flame structures and combustion performance.
Le *et al*.[109]	Methyl decanoate	Soot and OH distributions	Fuel-PLIF, OH-PLIF and soot-PLIF	To analyze the detail influence of jet-wall interaction on impinging flame development and soot formation.
Tang *et al*.[110]	PRF70	Natural combustion luminosity images and emission spectra of OH, CH, and CH_2O.	Multiple PLIF diagnostic methods	To study the effects of spray-wall impingement on flame propagation and UHC formation of gasoline PPC.
Tang *et al*.[111]	PRF70	Natural combustion luminosity images and emission spectra of OH, CH, and CH_2O.	Fuel-tracer PLIF, high-speed imaging, spectrometry and CH_2O/OH PLIF	The flame development and pollutants emission characteristics from different combustion stages in PPC.
Tripathi *et al*.[112]	PAO biodiesel	NO*x* emission	Exhaust gas analyzers	To study the effect of palm acid oil biodiesel on NO*x* emission fro m FWI in the automotive compression ignition engine.

advanced combustion technology with higher system efficiency and lower pollutant emissions, it is urgent and worthwhile to investigate characteristics of soot formation and evolution in FWI. It also facilitated to the optimization geometry design of various engines.

4.1 Soot characteristics in FWI of internal combustion engines

The production of unburned hydrocarbons was prevalently found in internal combustion engines due to the widespread existence of combustion chamber crevices, oil films absorption and desorption, flame quenching and etc. Among them, the formation of soot from FWI accounted for the dominant sources of UHC because the flame impingement was widely found in the confined volume combustors. Researchers were very interested in characteristics of soot in FWI and the relevant strategies to reduce soot formation in engines.[104-112] The analysis of these studies were shown in Table 3.

Most of the studies were carried out in various internal combustion engines. The optical accessible environment of engines and the utilization of multiple laser detection devices allowed researchers to directly observe soot behaviors from FWI in internal engines. Rusly *et al*.[107] emphatically studied effects of jet-wall and jet-jet interactions on flame structures and soot characteristics in an automotive-size optically accessible diesel engine. The flame boundary was obtained through the hydroxyl chemiluminescence imaging. The natural soot luminosity imaging was captured by a CMOS camera. In the research of Le *et al*.,[108] they were interested in the influences of FWI on the structure and development of diesel flames in a small-bore optical engine. Various combustion stages of the wall-interacting diesel flames were distinguished via OH-PLIF, fuel-PLIF and chemiluminescence imaging. In 2016, the same group of Le *et al*.[109] continued to investigate the behaviors of OH radical and soot particles in jet-wall interactions occurring in the optical diesel engine with the aid of various laser-based diagnostics techniques. To avoid the disturbance of other complex interactions such as jet-jet interactions, the single-hole nozzle was used in the experiment. Methyl decanoate which had the low-sooting propensity was chosen as the surrogate fuel to reduce laser attenuation. It was seen that the soot region tended to grow and flow along the bowl-wall surface. The existence of OH radical could oxidise soot particles and soot pockets shifted to be smaller in size and eventually disappeared.

To suppress soot formation in internal engines, the relevant strategies including the improvement of the nozzle spray geometry, injection pressure and etc. were proposed and tested in the research of soot characteristics from FWI. The properties of flame geometrical parameters and the ignition delay were obtained through flame imaging and OH chemiluminescence techniques to study the influence of included angle between two orifices on combustion performance.[104] Results showed that the nozzle spray configuration of the group-hole could effectively suppressed soot formation over wide engine loads due to the asymmetric flame structure. The effects of micro-hole nozzle and ultra-high injection pressure on properties of soot from the impinging diesel spray were experimentally investigated by Wang *et al*..[105] The parameter of KL which was proportional to the soot concentration was used to evaluate soot production. Both of soot temperature and the KL factor were measured according to two-color pyrometry. It exhibited that the flame-wall impingement obviously inhibited soot formation for the conventional nozzle. The decrease of soot concentration was observed with the augment of injection pressure. Less and smaller size soot was found in the impinging spray flame with the micro-hole nozzle at the injection pressure of 100 MPa. Kiplimo *et al*.[106] mainly studied the combustion and soot emission behaviors in a premixed charge compression ignition (PCCI) diesel engine under various spray impingement, injection parameters and EGR conditions. Less soot formation was found for both the late and early injection timings under the flame-wall impingement conditions. The decrease of soot concentration was more obvious with the adoption of EGR in the impinging spray flame. This phenomenon was attributed to the improvement of air-fuel mixing from the interaction between the flame and walls. In the research of Tripathi and Subramanian,[112] they found that palm acid oil (PAO) biodiesel which had higher spray penetration induced larger probability of wall impingement than that of base diesel. The strategy of retarding the injection timing obviously reduced the probability of wall impingement and the emission of NO*x*.

Based on the application of multiple laser diagnostics techniques in visual accessible engines, the variations of several major and intermediate species in FWI were also measured. To study the flame development and unburned hydrocarbon formation under the spray-wall impingement situation in an optical engine with low engine load, the combustion luminosity images and emission spectra which were obtained via multiple laser diagnostics measurements were presented.[110] The PLIF of formaldehyde was used to illustrate the UHC formation in gasoline partially premixed combustion (PPC). Results showed that the spray impingement reduced the combustion efficiency and the remains of CH_2O in the fuel-lean regions led to the production of UHC during the power stroke for fuel injection timing of -35°. Tang *et al*.[111] subsequently investigated the in-cylinder combustion processes of gasoline PPC and four different combustion stages were recognized and divided. The combustion emission spectra of various species including OH, CH, CH_2O, C_2 and CO were also offered. The "burn-out" stage was filled up by the spectra of OH and soot radiation.

Overall, the characteristics of soot formation in FWI have been widely analyzed (shown in Fig. 5) in diesel engines with different operating factors because the spray wall impingement prevalently occurring in internal combustion engines provided the well development of FWI. Some relevant strategies to reduce the soot formation in interaction between flame and walls were also studied in diesel engines. Various laser diagnostics measurements including OH-PLIF and fuel-PLIF were adopted to obtain the relevant flame structures and nature flame luminosity. Meanwhile, the distributions of other major and intermediate flame species were also measured. The properties of soot were extracted from the flame luminosity images which were captured because of soot radiation. In some extent, larger flame size represented the larger soot formation area and more soot concentration. These studies mainly quantitatively measured soot concentration variations in FWI. Other relevant characteristics of soot particles in FWI are also required in the future work.

4.2 Effects of various chamber geometries on soot formation

The above section of 4.1 presented that the flame impingement exhibited significant influence on soot properties in internal combustion engines by various laser diagnostics techniques. The reduction of soot formation was observed in impinging spray flames due to the improvement of fuel-air mixing in FWI. Based on the behaviors of soot in FWI, several researchers also proposed the utilization of various kinds of combustion chamber geometries which could intensify the interplay between flame and walls to reduce soot emission and improve combustion efficiency in internal engines.[113-122] Table 4 showed the summary of multiple strategies adopted in previous studies to improve soot emissions in flame-wall interactions.

The rapid development of computational fluid dynamics (CFD)

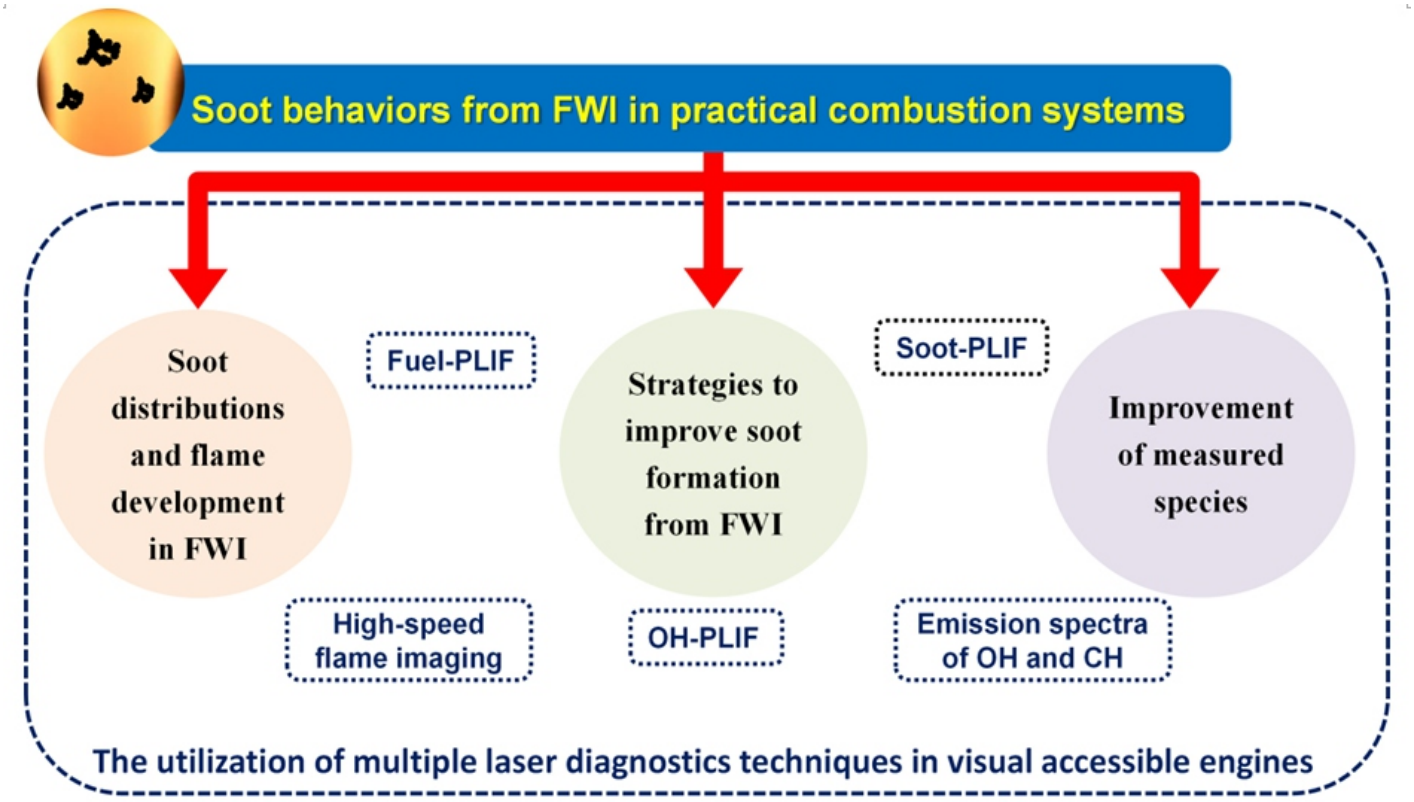

Fig. 5 The investigation of soot behaviors from FWI in practical combustion systems.

Table 4 The analysis of multiple strategies studied in previous research to modulate soot formation from flame-wall interactions in practical engines.

Relevant strategies to modulate soot formation		Analysis method		Analyzed species
		Simulated	Experimental	
The modification of piston bowl geometry	Changes of re-entrancy and central projection heights	Ref[113]	-	NO*x* and soot
	Variations of piston bowl diameter ratio and initial swirl ratio	Ref[116]	-	CO, NO and soot
	Changes of piston bowl depth and chamfered ring-land	Ref[119]	-	NO*x*, soot, HC and CO
The adoption of swirl combustion system	Analysis of a new swirl chamber combustion system	Ref[114]	-	NO and soot
	The adoption of forced swirl combustion system (FSCS).	Ref[115]	-	NO and soot
	The adoption of lateral swirl combustion system (LSCS).	Ref[122]	Ref[117], Ref[118] and Ref[120]	NO*x* and soot
	The investigation of a double swirl combustion system (DSCS).	-	Ref[117] and Ref[118]	NO*x* and soot
	Proposal of a novel multi-swirl combustion system (MSCS)	Ref[121]	Ref[121]	NO*x* and soot

offered researchers the convenient way to study the combustion processes occurring in internal engines with different geometries by numerical simulations. Several piston bowl geometry models with different re-entrancy and various central projection heights were simulated to study the effects of the new design of re-entrant piston bowl geometries on flow properties and pollutants emissions.[113] Results indicated that the optimization of piston bowl geometry could achieve 27% reduction of NO*x* emission and 85% decrease of soot concentration as compared to that of the baseline configuration. The influence of piston bowl diameter ratio and initial swirl ratio of a rectangular bowl on the engine performance and emissions was presented in the work of Abdul Gafoor *et al*..[116] The total thirty-five sorts of configurations with various d/D ratio and initial swirl ratio were considered and analyzed to acquire the optimum configuration with better combustion and pollutants emission behaviors. The augment of NO emission combined with the reduction of soot were found at the low d/D ratio because of the good combustion rate at TDC (top dead centre). They found that B3S1 was the best configuration for the minimum emission purpose and the case of B6S3 was the optimum design to gain the good combustion efficiency and low pollutants emissions. Considering that geometries of piston bowl significantly influenced the combustion and emission properties of engines, Kakaee *et al*.[119] numerically examined the reactivity controlled compression ignition (RCCI) engine performance and emissions with three different piston bowl geometries. Results showed that the influence of bowl profile on NO*x* emission was more obvious than that on UHC and CO emission at low engine speeds. The adoption of chamfered ring-land could suppress UHC formation at the conditions of chamfer sizes higher than 3 mm.

Except for investigations of variations of internal combustion engine geometries, several researchers devised novel combustion systems to enhance fuel and air mixtures and improve combustion performance. A new swirl chamber combustion system was proposed by Wei *et al*.,[114] and they simulated the mixture and combustion performance in the combustion chamber with different swirl ratios. Results presented that the lowest value of NO mass fraction was observed at swirl ratio of 0.8 and soot concentration was lowest at swirl ratio of 0.2. Overall, the better emission performance of the new combustion system was found at swirl ratio of 0.8. The numerical simulation to study the combustion and emission properties of the direct injection engine equipped with a new forced swirl combustion system (FSCS) was conducted by Su *et al*..[115] Compared to the emission characteristics of the traditional omega combustion system, the significant reduction of soot mass fraction was found in diesel engine with FSCS due to the improved fuel/air mixture formation at the full load condition. The discrepancy of soot and NO*x* emission from conventional combustion system and FSCS was not obvious at the lower load. To further investigate the mechanism of lateral swirl combustion system (LSCS) on combustion and emission characteristics, Li *et al*.[122] carried out numerical simulations to analyze the influence of LSCS configuration on combustion performance at 2500 r/min and full engine load. Results showed that the combustion chamber induced the favorable flow guidance and enhanced the fuel/air mixture process when the deviation angle of flow-guide ranged between 15-27°. The optimization configuration of the LSCS could achieve the reduction of soot emission by 69-75%.

The above mentioned above studies were just numerical simulations and an array of experiments were also conducted to test the emission and combustion characteristics of different chamber geometries. The combustion and emission performance of the single cylinder engine equipped with double swirl combustion system (DSCS) and lateral swirl combustion system were separately analyzed by Su *et al*.[117] to gain the better understanding of mechanism of forced swirl combustion system. Results showed that devices of DSCS and LSCS promoted the flame spread space and area compared to that of conventional combustion system. The better fuel consumption and less soot formation were found in LSCS than that in DSCS because of the better fuel/air mixing. The research of Li *et al*.[118] indicated that the utilization of LSCS could decrease 63.4-70.8% of soot formation and the configuration of LSCS has better application in practical diesel engines than that of DSCS because of good fuel consumption and low soot emission at the low excess air ratio. The spray and combustion properties of the wall-impinging jet with lateral swirl (LS) and current enveloping (ω) combustion systems in the constant volume combustion vessel were comparably investigated.[120] It was observed that more soot was formed at the late stage and the distribution of soot was mainly around the wall of the ω chamber. Whereas, the formation of soot was enhanced at the early stage and it distributed away from the wall in the LS chamber. Consequently, the soot from LS chamber was more easily mixed with air and oxidized. Li *et al*.[121] analyzed the combustion and pollutants emission characteristics of a novel multi-swirl combustion system (MSCS) from experimental and numerical aspects. The experimental results which obtained in the diesel engine showed that the soot emission from MSCS reduced 60% compared to that from the DSCS. The relevant simulation results exhibited that the reduction of soot emission in MSCS was attributed to the enlargement of the fuel diffusion space and the promotion of the fuel/air mixture.

Based on the fact that the interaction between fuel spray jets and wall surfaces could significantly affect the fuel diffusion around the combustor walls and further influence the engine performance, several researchers proposed various combustor configurations to improve the pollutants emission performance (shown in Fig. 6). Multifarious combustion systems were devised according to the forced swirl combustion phenomenon and they were analyzed via experiments and numerical simulations from the fuel consumption, NO*x* and soot emission aspects to acquire the optimum combustion system. The relevant information of flame structures and soot luminosity were also obtained with the use of various laser and optical diagnostics measurements in optical accessible diesel engines. The design of LSCS and DSCS could significantly reduce the fuel consumption and suppress soot formation because the utilization of various wall shapes enhanced the mixing of fuel and air. The results proved that these devices with good energy utilization and low soot emission had better application prospects in practical combustion systems.

4.3 Nanostructure of soot in flame-wall interactions

The effects of flame-wall interactions on soot properties from internal combustion engines were widely studied in aforementioned studies by laser diagnostics methods such as soot-PLII and etc. The measurement of soot area, soot volume fraction and optical thickness were obtained to get the information of soot spatial distributions in the boundary region near the wall surface. The obtained limited information just provided the coarse data of soot quantity because of the questionable assumption of soot particle optical properties. Recently, some researchers proposed the novel sampling method that acquired soot particles directly from diesel flames based on thermophoretic soot sampling techniques which were generally used in different laboratory flames.[123-127] Then more detailed knowledge of soot sizes and structures could be obtained with the help of transmission electron microscope (TEM). The analysis of soot structures including the physical dimensions of soot aggregates, primary particles and carbon lamella helped to gain the deep insight of soot formation and oxidation

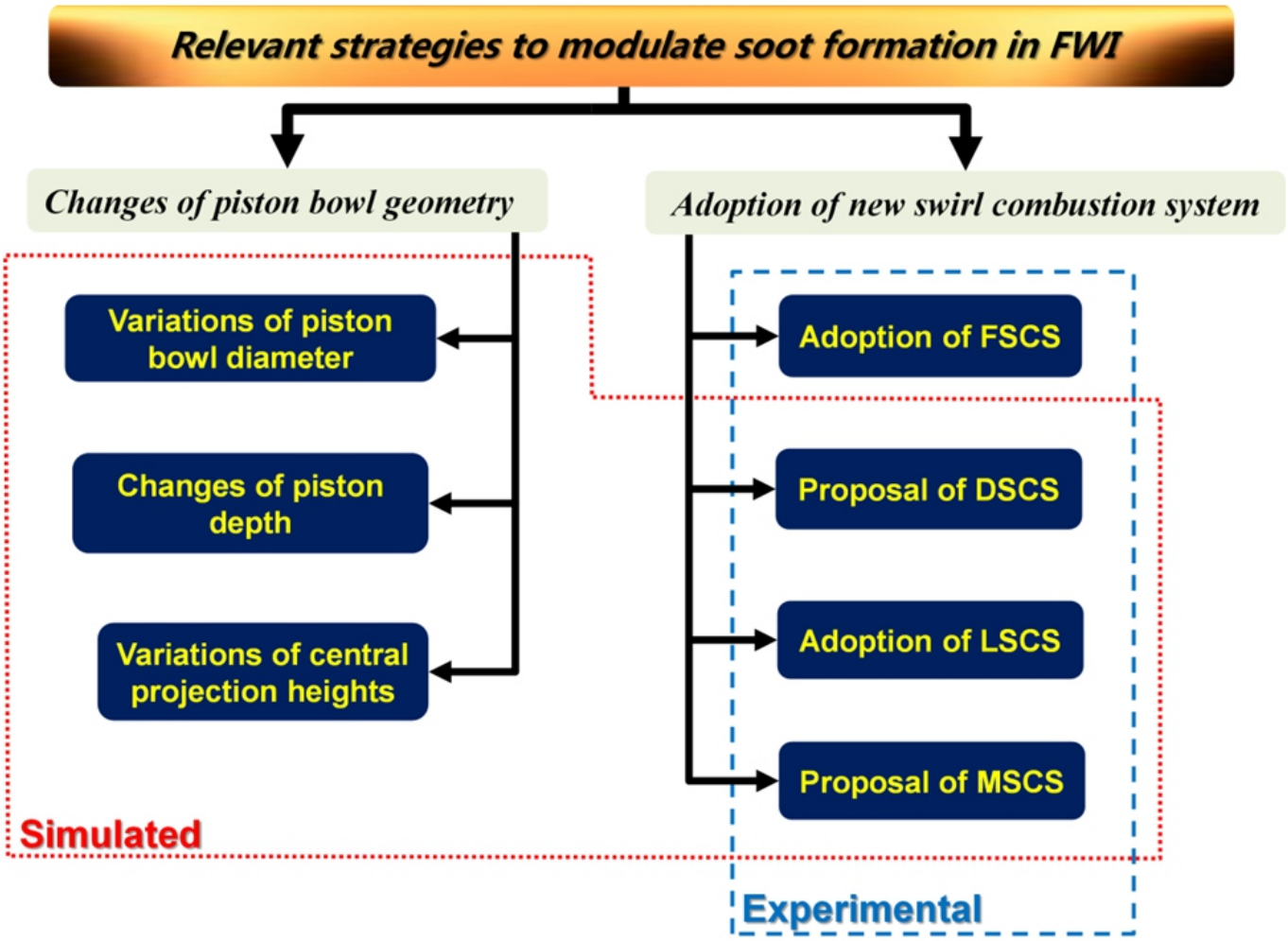

Fig. 6 The summary of relevant strategies adopted to modulate soot formation in FWI.

processes at various combustion stages in flame-wall interactions.

The combination of TEM images of soot particles from different locations and the statistics analysis method provided the detailed information of soot formation and evolution in FWI of practical engines. In the study of Zhang *et al*.,[123] soot samples from diesel flames were captured through the TEM gird probe which was installed on the combustor walls. The morphology of soot was examined by the TEM. Soot particles from different combustion stages were sampled and analyzed to acquire the effects of flame-wall interactions on soot particle morphology. The soot particle number concentration, size distribution and fractal morphology were analyzed with statistics methods. It showed that soot aggregates were more easily oxidized in flame-wall interactions and led to the increase numbers of small particles in the post-impingement stage because of the fragmentation of soot aggregates. More compacted soot particles were observed in the burn-out stage due to the further oxidation of soot. The morphological variations of soot particles from jet-to-jet variations and jet-jet interactions in single-cylinder diesel engine were experimentally investigated by Zhang *et al*.[127] with thermophoretic soot sampling and TEM imaging analyzing method. Results exhibited that soot sampled from jet-jet interactions presented higher particle number counts than that from the single-jets. Soot from the jet-jet interaction region was observed to be much smaller than those from single-jet head region. Few variations of soot sizes and fractal dimension were found for soot sampled from the in-flame and exhaust flues due to jet-jet interactions.

The information of soot nanostructures including fringe length, tortuosity and separation distances was acquired to evaluate soot internal structure variations in FWI. To get the deep understanding of soot size and structure variations in jet-jet interactions from diesel flames, soot samples from the diesel engine were imaged by TEM instruments to acquire soot morphology and nanostructures.[124] The crucial parameters of soot nanostructures such as fringe length, tortuosity and separation distances combined with primary particle diameter and fractal dimension were acquired. Compared to soot in the wall-impingement region, the faster initial growth of soot was found in the fuel-rich region due to jet-jet interaction. Moreover, the soot with larger aggregates and primary particles sampled in jet-jet interactions also presented the larger fringe separation distance and indicated higher particle reactivity. Zhang *et al*.[125] sampled soot particles in the small-bore diesel engine at five different locations via the soot sampling probe to investigate the soot formation processes in flame-wall interactions. The TEM images of soot from various locations showed that small soot particles with amorphous structures like precursors were found in the initial flame impingement region. These particles tended to be large and long–stretched aggregates as the soot travelled along the walls. The

typical core-shell structure was also observed at the downstream locations. At the further downstream place which located at the outer region of the flame, the size of soot aggregates decreased due to the intensive oxidation of hydroxyl radical. The same group of Zhang *et al.*[126] continued to analyze the influence of oxygenated biodiesel on soot formation in small-bore optical diesel engine. Compared to soot from traditional petroleum diesel, soot aggregates with less agglomerated and more stretched structures were found in methyl decanoate flames. The soot from methyl decanoate exhibited lower fringe separation distance and implied the more graphitized structures than those from petroleum diesel.

Except for the traditional investigation of soot concentration variations in FWI, the characteristics of soot particles from FWI such as size and structures which contributed to the improved understanding of soot formation and oxidation processes were studied and summerized in Fig. 7. The installment of sampling probes on the combustors walls combined with the utilization of TEM imaging devices provided researchers an opportunity to gain the essential knowledge of soot particle size and structures from multiple combustion stages in diesel engines. The laser diagnostics techniques were used to distinguish various combustion stages. The effects of flame-wall interactions on soot characteristics such as soot morphology, fractal dimension, primary particle diameter, and fringe parameters were also explicitly analyzed. Soot particles with precursor-like structures were mainly found in the initial impingement region. The more complex fractal structures and smaller size of soot were observed at the downstream region as the flame propagated along the wall surface. Meanwhile, the intensive oxidation of soot in the wall-jet head region diminished the tiny and simple particles and led to the fragmentation of large aggregates. The detailed information of soot morphology and nanoscale internal structures revealed the soot formation and evolution processes in FWI and it was also the supplement of previous studies.

Considering the wide existence of flame-wall interactions in practical combustion engines, many experiments were carried out in optical accessible diesel engines to examine the soot behaviors in the interplay between flame and walls with the aid of multiple laser-based diagnostics techniques. The relevant strategies to reduce soot formation in FWI under different operating engine conditions were also proposed. Taking advantage of the significant influence of FWI on soot formation behaviors, researchers proposed multifarious combustion systems such as MSCS and DSCS to modulate soot production and improve the combustion efficiency in confined combustion vessels because of the improvement of fuel/air mixture. To get deep insight of soot characteristics in FWI, the morphology and nanostructure of soot in flame-wall interactions were also studied through the thermophoretic sampling approaches and TEM imaging techniques. The evolution of soot morphology along the wall surface and the analysis of soot internal structure parameters illustrated soot formation and oxidation in FWI. As all of these studies were conducted in practical combustion systems, the transient flame condition combined with the complex combustion

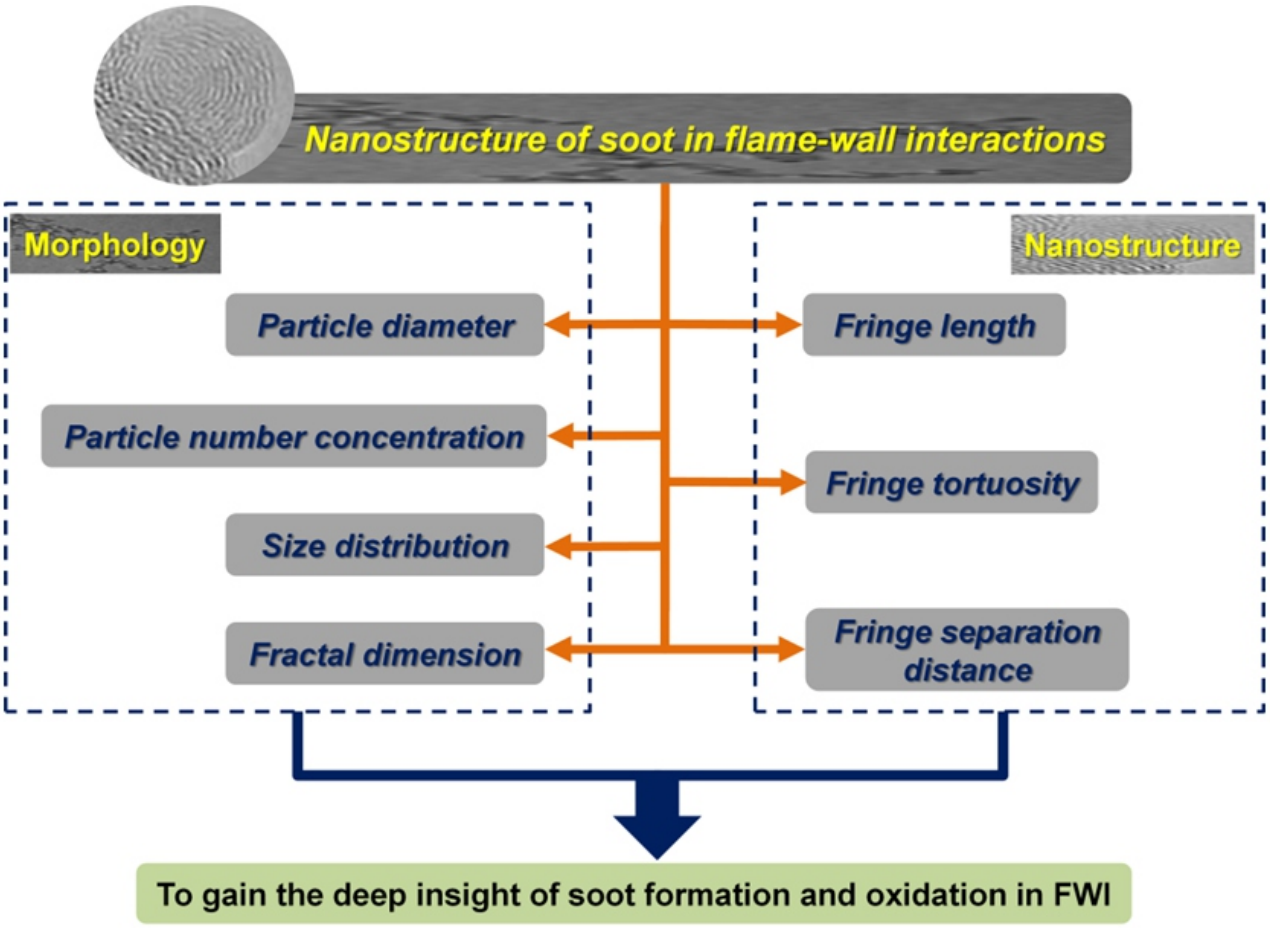

Fig. 7 The analysis of soot nanostructure from flame-wall interactions.

processes easily interfered the accuracy of sampling and measurement. In future work, more characteristics of soot in FWI from steady flames are urgent to be studied.

5. Soot characterisitcs in flat stabilized flames

The adoption of direct thermophoretic sampling approaches and TEM imaging device could offer the explicit knowledge of soot structural characteristics in FWI from diesel engines. However, the transient and unsteady flame environment where soot was sampled was easily influenced by other experimental parameters because of the complex combustion processes occurring in the confined combustion vessels. It was also difficult to separate flame-wall interaction from jet-jet or other complicated interactions occurring in diesel engines. To acquire more accurate and precise measurements, researchers adopted the burner-stabilized stagnation (BSS) flame configuration which could offer the steady flame and the well-defined flow rate boundary conditions to investigate soot particle size distribution functions (PSDF) and PAHs formation processes from the laboratory flames.[128-132]

The burner-stabilized stagnation flame configuration which combined the sampling probe with a water-cooled flat plate was introduced to examine the soot particle size distributions in ethylene/oxygen premixed flames.[128] The sampling probe was used to capture soot for mobility particle sizing. The stagnation plate above the burner could provide the steady flame and the strict definition of boundary conditions because of flame-wall interactions. The soot particle size distribution functions of various burner to stagnation surface distances were measured. Abid *et al*.[129] continued to study the evolution of nascent soot particle size distributions from laminar premixed n-dodecane flames via the similar BBS flame sampling approach. The variations of PSDF curves from n-dodecane flames were much similar to those from the previous ethylene flames. Compared to soot from ethylene flames, the nucleation mode was stronger in the n-dedecane flames. The experimental data of the PSDF of incipient soot obtained from BBS flame configuration was also offered to comparably study the influence of fuel structure and fuel bound oxygen on soot properties from butanol fuels.[130]

The distributions of major and intermediate species in BBS flames were also measured to validate relevant chemical mechanism and establish soot formation models. In the study of Saggese *et al*.,[131] the experimental data gained from the ethylene/oxygen premixed burner-stabilized stagnation flame was used to verify the predicted results including the soot volume fraction and soot size distributions from the model. It was found that the bimodal size distribution function of soot from the model was in a good agreement with observations from experiments. Kang *et al*.[132] examined the influence of dimethyl ether addition on PAHs and soot formation characteristics in ethylene premixed burner-stabilized flames. The distributions of flame temperatures, soot number density and soot particle diameters along different heights above the burner were performed. Results showed that the augment of soot volume fraction and the bimodal curve of PSDF which used to be unimodal in the post-flame region were found in the stagnation boundary layer. This phenomenon was ascribed to the intense flame-wall interactions which enhanced soot surface growth and condensation of PAHs. Meanwhile, the decrease of soot number density and the volume fraction were found with the increasing addition of DME in C_2H_4 premixed BSS flames.

The utilization of burner-stabilized flame configuration was mainly focused on the investigation of nascent soot particle size distribution functions from the various laminar premixed stagnation flames and the verification of relevant kinetic chemical mechanisms of soot formation. The presence of stagnation plate above the burner provided the stable flame environment and the rigorous flow rate boundary conditions because of the flame-wall interactions. The measurement of relevant soot size distribution variations were along the axis direction instead of the radial direction. More characteristics of soot from burner-stabilized stagnation flames along the radial direction are needed to further analyze the effects of flame-wall interplay on soot formation and oxidation processes.

6. Future prospective for pollutants emission studies from flame-wall interactions

The aforementioned investigations discussed in section 2, 3, 4 and 5 provided the multifarious insights of pollutants emission characteristics from laboratory and practical combustion systems (shown in Fig. 8). Judging from the aforementioned studies, limited information of distributions of major and intermediate species in the boundary layer which was important to gain the pollutants formation path was offered. There were few researchers deeply analyzing the kinetic mechanism of soot formation and examining soot internal structures variations from physical and chemical aspects in the flame-wall interactions. Moreover, the correlations between major and intermediate species and soot formed in flame-wall interactions were also unrevealed. Especially for the relevant fundamental combustion experiments and chemical kinetic soot formation models which involving soot formation and evolution characteristics in the interplay between the flame and walls were seriously scarce. It not only restricted the comprehension and understanding of soot formation processes with the presence of flame-wall interactions but also affected the development of new strategies to control pollutants emissions from various practical combustion appliances.

The essential effects of flame-wall interaction on pollutant emission characteristics were mainly via the reconstruction of chemical structures and flow fields of flames and the changes of combustion reaction paths which subsequently influenced the formation and evolvement of soot and other large PAHs. Thereby, there are several crucial fundamental scientific issues to be urgently resolved:

- The elaborate mole fraction distributions of more major and intermediate flames species in the boundary layer near the wall surface.
- The formation, evolution and distributions of soot in flame-wall interactions.
- The relevant soot formation chemical kinetic mechanism and model under the interplay between flame and walls.
- The correlations between PAH precursors and the physical and chemical characteristics of soot particles in flame-wall interactions.

More work should be done because of the complexity of the flame-wall interactions. The further investigation of pollutants emission from flame-wall interactions will improve the understanding of near-wall combustion phenomenon occurring in modern combustion systems. It will also provide the guideline for researchers and engineers to control and reduce soot formation in practical combustion devices from experimental and theoretical aspects and contribute to the promotion of fundamental combustion and pollutants control and the development of advanced combustion technologies.

7. Conclusion

This investigation of the pollutants emissions from FWI in fundamental and practical energy conversion systems principally concentrated on CO and soot aspects. The variations of CO mole fractions in various

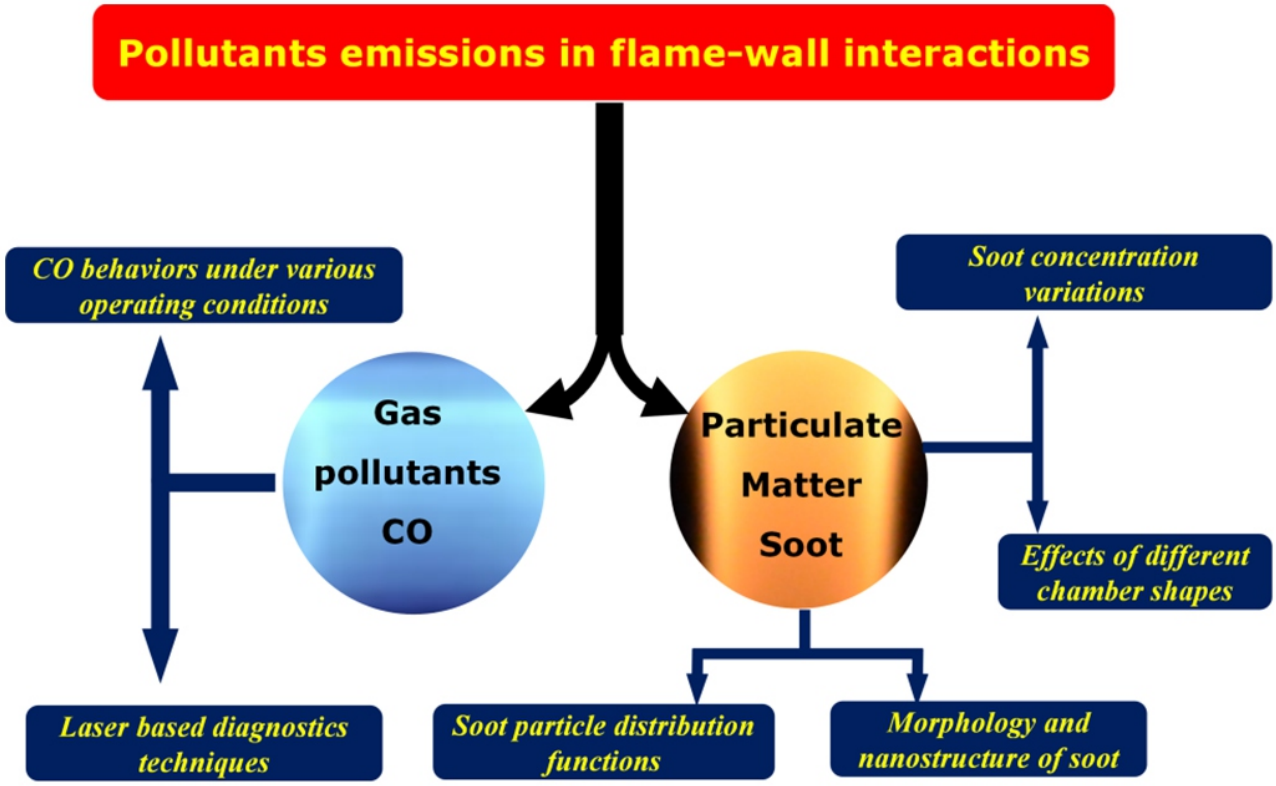

Fig. 8 The sketch of pollutants emissions in flame-wall interactions studied in previous research.

impinging flame configurations with different experimental parameters were presented. The local in-flame layer CO concentration distributions combined with the overall emission index of CO were adopted to emphasize the effects of flame-wall interactions on CO emission. Various laser based diagnostics techniques which could simultaneously measure multiple parameters and had the high spatial resolution were used to obtain the accurate and precise distributions of CO in the flame boundary layer near the wall surface. The studies of soot emissions from FWI were universally carried out in various diesel engines because of the prevalent existence of flame-wall interactions in internal combustion engines. Soot behaviors from FWI were presented and the relevant operating strategies to reduce soot formation were also proposed. Taking advantage of the influence of FWI on soot formation, multifarious combustion systems with different geometries were also designed and tested from experimental and numerical aspects to improve the combustion processes and reduce pollutants emissions. It helped to develop the optimum combustor configuration with the highest combustion efficiency and lowest soot emission. Moreover, the development of thermophoretic sampling method and TEM imaging devices allowed researchers to investigate morphology and nanostructure of soot from different locations of engine walls and to gain the profound understanding of soot formation and evolution in FWI. The soot particle size distribution functions from laboratory flames were measured through the stagnation plate which offered the stable flames and the rigorous boundary conditions due to flame-wall interaction. Several crucial scientific issues which were expected to be resolved were proposed at the end of this review. To conclude, there are a lot of work should be done in the future work to gain more knowledge of the essential effects of flame-wall interactions on pollutants emissions.

Acknowledgement

This work was supported by the National Natural Science Foundation of China (51822605, 51576100 and 51776181) and 333 Program of Jiangsu Province (BRA2017428).

Reference

1. A. Dreizler and B. Böhm, *P. Combust. Inst.*, 2015, **35**, 37-64.
2. T. Poinsot and D. Veynante, *Theoretical and Numerical Combustion*, Edwards, Philadelphia, 2005.
3. H. W. Zhang and Z. Chen, *Combust. Theor. Model.*, 2013, **17**, 682-686.
4. G. Bruneaux, T. Poinsot and J. H. Ferziger, *J. Fluid. Mech.*, 1997, **349**, 191-219.
5. A. Gruber, R. Sankaran, E. R. Hawkes and J. H. Chen, *J. Fluid. Mech.*, 2010, **658**, 5-32.
6. G. Desoutter, B. Cuenot, C. Habchi and T. Poinsot, *P. Combust. Inst.*, 2005, **30**, 259-266.
7. J. Jiménez, *Annu. Rev. Fluid. Mech.*, 2004, **36**, 173-196.
8. K. L. Edwards and M. J. Norris, *Mater. Design*, 1999, **20**, 245-252.
9. J. Daou and M. Matalon, *Combust. Flame*, 2002, **128**, 321-339.
10. K. T. Kim, D. H. Lee and S. Kwon, *Combust. Flame*, 2006, **146**, 19-28.
11. R. Sadanandan, D. Markus, R. Schießl, U. Maas, J. Olofsson, H. Seyfried, M. Richter and M. Aldén, *P. Combust. Inst.*, 2007, **31**, 719-726.
12. X. L. Zhang, L. H. Hu, M. A. Delichatsios and J. P. Zhang, *P. Combust. Inst.*, 2018, https://doi.org/10.1016/j.proci.2018.06.203.
13. H. W. Ding and J. G. Quintiere, *Fire Safety J.*, 2012, **52**, 25-33.
14. B. Y. Lattimer, C. Mealy and J. Beitel, *Fire Technol.*, 2013, **49**, 269-291.
15. X. C. Zhang, H. W. Tao, W. B. Xu, X. Z. Liu, X. D. Li, X. L. Zhang and L. H. Hu, *Combust. Flame*, 2017, **176**, 349-357.
16. Z. H. Gao, J. Ji, H. X. Wan, K. Y. Li and J. H. Sun, *P. Combust. Inst.*, 2015, **35**, 2657-2664.
17. Y. D. Wang, A. Vouros, J. P. Zhang and M. A. Delichatsios, *J. Loss Prevent*

Proc., 2017, **49**, 652-659.
18. O. Deutschmann, L. I. Maier, U. Riedel, A. H. Stroemman and R. W. Dibble, *Catal. Today*, 2000, **59**, 141-150.
19. C. Appel, J. Mantzaras, R. Schaeren, A. Inauen, N. Tylli, M. Wolf, T. Griffin, D. Winkler and R. Carroni, *P. Combust. Inst.*, 2005, **30**, 2509-2517.
20. C. Appel , J. Mantzaras, R. Schaeren, R. Bombach, A. Inauen, B. Kaeppeli, B. Hemmerling and A. Stampanoni, Combust. Flame, 2002, **128**, 340-368.
21. R. Schwiedernoch, S. Tischer, C. Correa and O. Deutschmann, *Chem. Eng. Sci.*, 2003, **58**, 633-642.
22. R. W. Sidwell, H. Y. Zhu, R. J. Kee and D. T. Wickham, *Combust. Flame*, 2003, **134**, 55-66.
23. G. D. Falco, M. Commodo, M. Barra, F. Chiarella, A. D'Anna, A. Aloisio, A. Cassinese and P. Minutolo, *Synthetic Met.*, 2017, **229**, 89-99.
24. C. T. Chong, W. H. Tan, S. L. Lee, W. W. F. Chong, S. S. Lam and A. Valera-Medina, *Mater. Chem. Phys.*, 2017, **197**, 246-255.
25. I. S. Bayer, A. J. Davis, E. Loth and A. Steele, *Mater. Today Commun.*, 2015, **3**, 57-68.
26. I. S. Bayer, A. J. Davis and A. Biswas, *RSC Adv.*, 2014, **4**, 264-268.
27. K. Maruta, *P. Combust. Inst.*, 2011, **33**, 125-150.
28. A. D. Stazio, C. Chauveau, G. Dayma and P. Dagaut, *Exp. Therm. Fluid Sci.*, 2016, **73**, 79-86.
29. G. Pizza, C. Frouzakis, J. Mantzaras, A. G. Tomboulides and K. Boulouchos, *Combust. Flame*, 2008, **152**, 433-450.
30. K. Maruta, K. Takeda, J. Ahn, K. Borer, L. Sitzki, P. D. Ronney and O. Deutschmann, *P. Combust. Inst.*, 2002, **29**, 957-963.
31. C. M. Miesse, R. I. Masel, C. D. Jensen, M. A. Shannon and M. Short, *Aiche. J.*, 2004, **50**, 3206-3214.
32. K Maruta, T. Kataoka, N. I. Kim, S. Minaev and R. Fursenko, *P. Combust. Inst.*, 2005, **30**, 2429-2436.
33. W. A. Daniel, *P. Combust. Inst.*, 1957, **6**, 886-894.
34. J. B. Heywood, *Symp. Combust.*, 1975, **15**, 1191-1211.
35. R. Ljones, *Combust. Sci. Technol.*, 1997, **129**, 185-195.
36. M. C. Drake and D. C. Haworth, *P. Combust. Inst.*, 2007, **31**, 99-124.
37. A. H. Epstein, *Combust. Flame*, 2012, **159**, 1791-1792.
38. W. Schwarz, S. Schwub, K. Quering, D. Wiedmann, H. W. Höppel and M. Göken, *CEAS Space J.*, 2011, **1**, 83-97.
39. Z. J. Sroka, *J. Therm. Anal. Calorim.*, 2012, **110**, 51-58.
40. U. Stopper, W. Meier, R. Sadanandan, M. Stöhr, M. Aigner and G. Bulat, *Combust. Flame*, 2013, **160**, 2103-2118.
41. Y. Huang and V. Yang, *Combust. Flame*, 2004, **136**, 383-389.
42. S. S. Hou, S. S. Yang, S. J. Chen and T. H. Lin, *Combust. Flame*, 2003, **132**, 58-72.
43. P. Kuntikana and S. V. Prabhu, *Appl. Therm. Eng.*, 2016, **99**, 905-918.
44. V. Hindasageri, R. P. Vedula and S. V. Prabhu, *Int. J. Heat Mass Tran.*, 2014, **77**, 185-193.
45. J. Y. Jiang, T. Q. Wu, J. X. Yi and X. Jiang, *Energy Procedia.*, 2015, **66**, 325-328.
46. M. Jarray, K. Chetehouna, N. Gascoin and F. Bey, *Int. J. Therm. Sci.*, 2016, **107**, 184-195.
47. S. Lee and C. Park, *Int. J. Therm. Sci.*, 2012, **51**, 102-111.
48. C. Csernyei and A. G. Straatman, *Appl. Therm. Eng.*, 2016, **105**, 290-303.
49. V. M. Sauer and D. Dunn-Rankin, *P. Combust. Inst.*, 2016, **36**, 1411-1419.
50. J. Fu, C. W. Leung, Z. H. Huang, Y. Zhang and C. S. Cheung, *Exp. Therm. Fluid. Sci.*, 2016, **70**, 335-340.
51. H.S. Zhen, C. W. Leung, C. S. Cheung and Z. H. Huang, *Int. J. Heat Mass Tran.*, 2016, **92**, 807-814.
52. H. S. Zhen, C. W. Leung and C. S. Cheung, *Int. J. Hydrogen Energ.*, 2013, **38**, 6874-6881.
53. H. S. Zhen, C. W. Leung, C. S. Cheung and Z. H. Huang, *Int. J. Heat Mass Tran.*, 2016, **92**, 807-814.
54. Z. Zhao, T. T. Wong and C. W. Leung, *Int. J. Heat Mass Tran.*, 2004, **47**, 5021-5031.
55. L. L. Dong, C. S. Cheung and C. W. Leung, *Int. J. Heat Mass Tran.*, 2013, **56**, 360-369.
56. P. Kuntikana and S. V. Prabhu, *Int. J. Therm. Sci.*, 2017, **111**, 409-422.
57. Z. U. Ahmed, Y. M. Al-Abdeli and F. G. Guzzomi, *Int. J. Heat Mass Tran.*, 2016, **102**, 991-1003.
58. L. L. Dong, C. S. Cheung and C. W. Leung, *Int. J. Heat Mass Tran.*, 2002, **45**, 979-992.
59. L. L. Dong, C. S. Cheung and C. W. Leung, *Int. J. Heat Mass Tran.*, 2007, **50**, 5124-5138.
60. S. S. Hou and Y. C. Ko, *Energ. Convers. Manage.*, 2004, **45**, 1583-1595.
61. M. R. Morad, A. Momeni, E. Ebrahimi Fordoei and M. Ashjaee, *Int. J. Therm. Sci.*, 2016, **110**, 229-240.
62. Z. L. Wei, H. S. Zhen, C. W. Leung, C. S. Cheung and Z. H. Huang, *Int. J. Hydrogen Energ.*, 2015, **40**, 15723-15731.
63. S. Chander and A. Ray, *Int. J. Heat Mass Tran.*, 2011, **54**, 1179-1186.
64. L. L. Dong, C. W. Leung and C. S. Cheung, *Int. J. Heat Mass Tran.*, 2003, **46**, 113-125.
65. H. S. Zhen, C. W. Leung and C. S. Cheung, *Appl. Therm. Eng.*, 2012, **36**, 386-392.
66. D. Mira Martinez, X. Jiang, C. Moulinec and D. R. Emerson, *Fuel*, 2013, **103**, 646-662.
67. D. Mira Martinez and X. Jiang, *Fuel*, 2013, **109**, 285-296.
68. R. Viskanta, *Exp. Therm. Fluid Sci.*, 1993, **6**, 111-134.
69. C. E. Baukal and B. Gebhart, *Combust. Sci. Technol.*, 1995, **104**, 339-357.
70. C. E. Baukal and B. Gebhart, *Combust. Sci. Technol.*, 1995, **104**, 359-385.
71. S. Chander and A. Ray, *Energ. Convers. Manage.*, 2005, **46**, 2803-2837.
72. J. W. Wohr, J. Seyed-Yagoobi and R. H. Page, *Combust. Flame*, 1996, **106**, 69-80.
73. P. Popp and M. Baum, *Combust. Flame*, 1997, **108**, 327-348.
74. D. P. Mishra, *Fuel*, 2004, **83**, 1743-1748.
75. L. K. Sze, C. S. Cheung and C. W. Leung, *Int. J. Heat Mass Tran.*, 2004, **47**, 3119-3129.
76. U. Makmool, S. Jugjai, S. Tia, P. Vallikul and B. Fungtammasan, *Energy*, 2007, **32**, 1986-1995.
77. C. Saha, R. Ganguly and A. Datta, *Exp. Heat Transfer*, 2008, **21**, 169-187.
78. H. B. Li, H. S. Zhen, C. W. Leung and C. S. Cheung, *Int. J. Heat Mass Tran.*, 2010, **53**, 4176-4184.
79. H. B. Li, H. S. Zhen, C. W. Leung and C. S. Cheung, *Int. J. Heat Mass Tran.*, 2011, **54**, 625-635.
80. H. S. Zhen, C. W. Leung and C. S. Cheung, *Appl. Energ.*, 2011, **88**, 1629-1634.
81. Y. S. Choy, H. S. Zhen, C. W. Leung and H. B. Li, *Appl. Energ.*, 2012, **91**, 82-89.
82. U. Makmool, S. Jugjai and S. Tia, *Fuel*, 2013, **112**, 254-262.
83. P Muthukumar and P. I. Shyamkumar, *Fuel*, 2013, **112**, 562-566.
84. H. S. Zhen, C. W. Leung and T. T. Wong, *Fuel*, 2014, **119**, 153-156.
85. A. R. Tajik and V. Hindasageri, *Appl. Therm. Eng.*, 2015, **89**, 534-544.
86. N. K. Mishra, S. C. Mishra and P. Muthukumar, *Appl. Therm. Eng.*, 2015, **89**, 44-50.
87. S. Panigraphy, N. K. Mishra, S. C. Mishra and P. Muthukumar, *Energy*, 2016, **95**, 404-414.
88. H. S. Zhen, Z. L. Wei, C. W. Leung, C. S. Cheung and Z. H. Huang, *Int. J. Hydrogen. Energ.*, 2016, **41**, 2087-2095.
89. Z. L. Wei, H. S. Zhen, C. W. Leung, C. S. Cheung and Z. H. Huang, *Fuel*, 2017, **195**, 1-11.
90. N. K. Mishra and P. Muthukumar, *Appl. Therm. Eng.*, 2018, **129**, 482-489.
91. A. V. Mokhov, A. P. Nefedov, B. V. Rogov, V. A. Sinel'shchikov, A. D. Usachev and A. V. Zobnin, *Combust. Flame*, 1999, **119**, 161-173.
92. T. Fuyuto, H. Kronemayer, B. Lewerich, J. Brübach, T. Fujikawa, K. Akihama, T. Dreier and C. Schulz, *Exp. Fluids*, 2010, **49**, 783-795.
93. A. Singh, M. Mann, T. Kissel, J. Brübach and A. Dreizler, *Flow Turbul. Combust.*, 2013, **90**, 723-739.
94. M. Mann, C. Jainski, M. Euler, B. Böhm and A. Dreizler, *Combust. Flame*, 2014, **161**, 2371-2386.
95. Y. C. Chien, D. Escofet-Martin and D. Dunn-Rankin, *Combust. Flame*, 2016, **174**, 16-24.

96. S. Ganter, A. Heinrich, T. Meier, G. Kuenne, C. Jainski, M. Rißmann M, A. Dreizler and J. Janicka, *Combust. Flame,* 2017, **186**, 299-310.
97. C. Jainski, M. Rißmann, B. Böhm, J. Janicka and A. Dreizler, *Combust. Flame,* 2017, **183**, 271-282.
98. A. Bohlin, C. Jainski, B. D. Patterson, A. Dreizler and C. Kliewer, *P. Combust. Inst.,* 2017, **36**, 4557-4564.
99. P. Versailles, A. Durocher, G. Bourque and J. M. Bergthorson, *P. Combust. Inst.,* 2018, http://doi.org/10.1016/j.proci.2018.05.060.
100. T. Häber and R. Suntz, *Int. J. Heat Fluid Fl.,* 2018, **69**, 95-105.
101. H. Kosaka, F. Zentgraf, A. Scholtissek, L. Bischoff, T. Häber, R. Suntz, B. Albert, C. Hasse and A. Dreizler, *Int. J. Heat Fluid Fl.,* 2018, **70**, 181-192.
102. S. Ganter, C. Straβacker, G. Kuenne, T. Meier, A. Heinrich, U. Maas and J. Janicka, *Int. J. Heat Fluid Fl.,* 2018, **70**, 259-270.
103. A. Heinrich, S. Ganter, G. Kuenne, C. Jainski, A. Dreizler and J. Janicka, *Flow Turbul. Combust.,* 2018, **100**, 535-559.
104. J. Gao, S. Moon, Y. Y. Zhang, K. Nishida and Y. Matsumoto, *Combust. Flame,* 2009, **156**, 1263-1277.
105. X. G. Wang, Z. H. Huang, W. Zhang, O. A. Kuti and K. Nishida, *Appl. Energ.*, 2011, **88**, 1620-1628.
106. R. Kiplimo, E. Tomita, N. Kawahara and S. Yokobe, *Appl. Therm. Eng.,* 2012, **37**, 165-175.
107. A. M. Rusly, M. K. Le, S. Kook and E. R. Hawkes, *Fuel,* 2014, **125**, 1-14.
108. M. K. Le, S. Kook and E. R. Hawkes, *Fuel,* 2015, **140**, 143-155.
109. M. K. Le, R. L. Zhang, L. Z. Rao, S. Kook and E. R. Hawkes, *Fuel,* 2016, **166**, 320-332.
110. Q. L. Tang, H. F. Liu, M. K. Li and M. F. Yao, *Appl. Energ.,* 2017, **185**, 708-719.
111. Q. L. Tang, H. F. Liu, M. K. Li, M. F. Yao and Z. S. Li, *Combust. Flame,* 2017, **177**, 98-108.
112. S. Tripathi and K. A. Subramanian, *Appl. Therm. Eng.,* 2018, **142**, 241-254.
113. B. V. V. S. U. Prasad, C. S. Sharma, T. N. C. Anand and R. V. Ravikrishna, *Appl. Energ.*, 2011, **88**, 2355-2367.
114. S. L. Wei, F. H. Wang, X. Y. Leng, X. Liu and K. P. Ji, *Energ. Convers. Manage.*, 2013, **75**, 184-190.
115. L. W. Su, X. R. Li, Z. Zhang and F. S. Liu, *Energ. Convers. Manage.*, 2014, **86**, 20-27.
116. C. P. Abdul Gafoor and R. Gupta, *Energ. Convers. Manage.*, 2015, **101**, 541-551.
117. L. W. Su, X. R. Li, X. He and F. S. Liu, *Energ. Convers. Manage.*, 2015, **106**, 826-834.
118. X. R. Li, H. Q. Zhou, L. W. Su, Y. L. Chen, Z. Y. Qiao and F. S. Liu, *Fuel*, 2016, **184**, 672-680.
119. A. H. Kakaee, A. Nasiri-Toosi, B. Partovi and A. Paykani, *Appl. Therm. Eng.*, 2016, **102**, 1462-1472.
120. X. R. Li, W. Yang, L. W. Su and F. S. Liu, *Appl. Therm. Eng.*, 2017, **123**, 7-18.
121. X. R. Li, Z. Y. Qiao, L. W. Su, X. L. Li and F. S. Liu, *Appl. Therm. Eng.*, 2017, **115**, 1203-1212.
122. X. R. Li, Y. L. Chen, L. W. Su and F. S. Liu, *Fuel*, 2018, **224**, 644-660.
123. R. L. Zhang and S. Kook, *Combust. Flame*, 2015, **162**, 2720-2728.
124. M. K. Le, Y. L. Zhang, R. L. Zhang, L. Z. Rao, S. Kook, Q. N. Chan and E. R. Hawkes, *P. Combust. Inst.,* 2017, **36**, 3559-3566.
125. Y. L. Zhang, D. Kim, L. Z. Rao, R. L. Zhang, S. Kook, K. S. Kim and C. B. Kweon, *Combust. Flame*, 2017, **185**, 278-291.
126. Y. L. Zhang, R. L. Zhang, L. Z. Rao, D. Kim and S. Kook, *Fuel,* 2017, **194**, 423-435.
127. R. L. Zhang, Y. L. Zhang and S. Kook, *Combust. Flame,* 2017, **176**, 377-390.
128. A. D. Abid, J. Camacho, D. A. Sheen and H. Wang, *Combust. Flame,* 2009, **156**, 1862–1870.
129. A. D. Abid, J. Camacho, D. A. Sheen and H. Wang, *Energ. Fuel,* 2009, **23**, 4286–4294.
130. J. Camacho, S. Lieb and H. Wang, *P. Combust. Inst.,* 2013, **34**, 1853–1860.
131. C. Saggese, S. Ferrario, J. Camacho, A. Cuoci, A. Frassoldati, E. Ranzi, H. Wang and T. Faravelli, *Combust. Flame,* 2015, **162**, 3356-3369.
132. Y. H. Kang, Y. M. Sun, X. F. Lu, X. L. Gou, S. C. Sun, J. Yan, Y. F. Song, P. Y. Zhang, Q. H. Wang and X. Y. Ji, *Energy*, 2018, **150**, 709-721.